

ENVIRONMENTAL INTERPRETATION OF THE UPPER
3C , THE 4R, AND THE LOWER 4E MEMBERS OF THE HELIKIAN-AGED
PARRY BAY FORMATION, BATHURST INLET, N.W.T.

by

Barbara J. Tilley

Submitted in partial fulfillment of the
requirements for the degree of
Bachelor of Science (Honours)

at

Dalhousie University
Halifax, Nova Scotia

1979



DEPARTMENT OF GEOLOGY
DALHOUSIE UNIVERSITY
HALIFAX, NOVA SCOTIA
CANADA
B3H 4J1

DALHOUSIE UNIVERSITY, DEPARTMENT OF GEOLOGY

B.Sc. HONOURS THESIS

Author: Barbara J. Tilley

Title: Environmental Interpretation of the Upper 3C, the 4R, and the Lower 4E Members of the Helikian-aged Parry Bay Formation, Bathurst Inlet, N.W.T.

Permission is herewith granted to the Department of Geology, Dalhousie University to circulate and have copied for non-commercial purposes, at its discretion, the above title at the request of individuals or institutions. The quotation of data or conclusions in this thesis within 5 years of the date of completion is prohibited without the permission of the Department of Geology, Dalhousie University, or the author.

The author reserves other publication rights, and neither the thesis nor extensive extracts from it may be printed or otherwise reproduced without the authors written permission.

Signature of author

Date: March 19, 1979

Copyright 1979

Distribution License

DalSpace requires agreement to this non-exclusive distribution license before your item can appear on DalSpace.

NON-EXCLUSIVE DISTRIBUTION LICENSE

You (the author(s) or copyright owner) grant to Dalhousie University the non-exclusive right to reproduce and distribute your submission worldwide in any medium.

You agree that Dalhousie University may, without changing the content, reformat the submission for the purpose of preservation.

You also agree that Dalhousie University may keep more than one copy of this submission for purposes of security, back-up and preservation.

You agree that the submission is your original work, and that you have the right to grant the rights contained in this license. You also agree that your submission does not, to the best of your knowledge, infringe upon anyone's copyright.

If the submission contains material for which you do not hold copyright, you agree that you have obtained the unrestricted permission of the copyright owner to grant Dalhousie University the rights required by this license, and that such third-party owned material is clearly identified and acknowledged within the text or content of the submission.

If the submission is based upon work that has been sponsored or supported by an agency or organization other than Dalhousie University, you assert that you have fulfilled any right of review or other obligations required by such contract or agreement.

Dalhousie University will clearly identify your name(s) as the author(s) or owner(s) of the submission, and will not make any alteration to the content of the files that you have submitted.

If you have questions regarding this license please contact the repository manager at dalspace@dal.ca.

Grant the distribution license by signing and dating below.

Name of signatory

Date

TABLE OF CONTENTS

	Page
LIST OF FIGURES	i
LIST OF PLATES	ii
LIST OF TABLES	iv
ABSTRACT	v
CHAPTER 1 - INTRODUCTION	1
Location and Access	1
Previous Work	1
Regional Geology	3
Purpose of Thesis	5
Field Methods	8
Terminology	10
Acknowledgements	12
CHAPTER 2 - FIELD DESCRIPTION OF UNITS	13
Unit 3C ₁	13
Unit 3C ₂ Coarse-grained Doloarenite	17
Unit 3C ₃	19
Unit 4R ₁ , Red Shale	20
Unit 4R ₂ , Mudstone-Dolosiltite Strata	22
Unit 4R ₃ , Intraclastic Strata	23
Unit 4R ₄ ,	27
Base of Stromatolitic Complex	29
Sub-circular SH-V	29
Elongate SH-V	37
SH-V with Shale Partings	39
Red SH-V	40
Branching SH-V	40
Isolated Stromatolitic Mound	42
Channel Deposits	45
Unit 4E Bioherms	47
CHAPTER 3 - LABORATORY ANALYSES	52
Cut Slabs	52
Polished Thin Sections	52
Calcite Staining	53
Insoluble Residue	54

	Page
Wet Chemical Analyses	57
X-ray Diffraction	59
DISCUSSION OF LABORATORY RESULTS	60
Insoluble Residue	60
Ca/Mg Ratio	62
Total Iron	64
Total Analysis Percentage	66
CHAPTER 4 - ENVIRONMENTAL INTERPRETATION	67
Units 3C ₁ and 3C ₂	67
Low Energy Environments	67
Medium-Energy Environments	68
Unit 3C ₃	69
Units 4R ₁ , 4R ₂ and 4R ₃ , Shale, Dolosiltite and Intraclasts	71
Deep-Water	73
Low Supratidal	74
Intertidal	75
Unit 4R ₄	76
Deep-Water Stromatolites	76
Shallow-Water Stromatolites	78
Unit 4E	83
CHAPTER 5 - CONCLUSIONS	84
REFERENCES	86
APPENDICES	88

LIST OF FIGURES

	Page
FIGURE 1. Map showing location of the study area.	2
FIGURE 2. Distribution of the various members of the Parry Bay Formation, in the Melville Sound Area.	4
FIGURE 3. Fence diagram of the study section, showing the vertical succession of the various lithosomes and their lithic correlation.	14
FIGURE 4. Map of the study section, showing locations of the top of Unit $4R_3$, in each measured section.	15
FIGURE 5. Composite schematic cross-section of Units $3C_1$ to $4R_3$.	16
FIGURE 6. Composite schematic cross-section of Unit $4R_4$.	31
FIGURE 7. Bar graph of insoluble residues, indicating the uncertainty range, for each sample.	55
FIGURE 8. Fence diagram showing the stratigraphic position of analyzed samples, and their insoluble residue percentages.	56
FIGURE 9. Plot of Ca mole percent versus Mg mole percent, for the thirty samples.	65
FIGURE 10. Plot of Fe_2O_3 weight percent versus Al_2O_3 weight percent, for the thirty analyzed samples.	65
FIGURE 11. Schematic diagram of the depositional environment interpreted from the study section.	85

LIST OF PLATES

	Page
PLATE 1. Plan view of a low-domal stromatolite in Unit 3C ₁ .	18
PLATE 2. Ridges on the bedding surface of reddish-brown, coarse-grained dolarenites, Unit 3C ₃ .	21
PLATE 3. Stratum with convex-upwards laminations underlain and overlain by shale, unit 4R ₂ , section F.	25
PLATE 4. Horizontally-oriented, columnar stromatolite, located immediately to the left of laminations in Plate 3.	25
PLATE 5. Unit 4R ₃ (outlined by dashed lines).	26
PLATE 6. Unit 4R ₃ (outlined by dashed lines), underlain by shale, interbedded with fine-grained dolarenite, and overlain by sub-circular SH-V.	26
PLATE 7. Close-up of an intraclastic stratum, unit 4R ₃ .	28
PLATE 8. Green and red weathering, low-domal stromatolites, evolving from slightly undulating medium-grained dolarenites.	32
PLATE 9. Basal columnar stromatolite, linked at its base but expanding upwards to form a domed-shape top.	32
PLATE 10. Plan view of sub-circular columnar stromatolites, appearing as small domes protruding above the inter-stromatolite sediment.	34
PLATE 11. Sub-circular columnar stromatolite with a central core.	35
PLATE 12. A vertical cross-section of the central core of a sub-circular columnar stromatolite.	35
PLATE 13. Plan view of very elongate columnar stromatolites.	36
PLATE 14. Cross-section of elongate columnar stromatolites.	36

	Page
PLATE 15. Cross-section of elongate columnar stromatolites.	38
PLATE 16. Elongate pseudo-columnar stromatolites, growing at angles of 15-28° from the vertical.	38
PLATE 17. Sub-vertical intraclasts between red SH-V (section M).	41
PLATE 18. Dark red, branching SH-V.	43
PLATE 19. Low-domal, close-linked stromatolites evolving into narrow, vertical, pseudo-columnar stromatolites.	44
PLATE 20. Channel deposit in section N, showing beds pinching out, and dipping towards, the mound of sub-circular and elongate columnar stromatolites to the left.	44
PLATE 21. Channel deposit from section N.	46
PLATE 22. Thin-bedded to laminated, red mudstone and fine-grained, green doloarenite are sharply overlain by very flat parallel beds of medium-grained doloarenite.	46
PLATE 23. Cracks on the top surface of mudstone strata.	48
PLATE 24. Bioherm of Unit 4E, section O.	49
PLATE 25. Plan view of very elongate, columnar stromatolites on the top surface of the unit 4E bioherms in Plate 22.	49
PLATE 26. Cross-sectional view of a portion of the upper part of the bioherm.	50

LIST OF TABLES

	Page
TABLE 1. Summary of the stratigraphy of the Bathurst Inlet Area (from Campbell, 1979).	6
TABLE 2. Dimensions of stromatolites in Unit 4R ₄ .	30
TABLE 3. Tabulated results of whole rock chemical analyses.	58
TABLE 4. Relative abundances of minerals in Sample K1 (by x-ray diffraction).	59

ABSTRACT

A stromatolitic, clastic, dolomite-mudstone section, within the central portion of the Parry Bay Formation, Bathurst Inlet, N.W.T., is described. The section is divided into seven lithological units, each of which are described and interpreted using field and laboratory data. Laboratory data include rock slabs, thin sections, calcite staining, insoluble residues, wet chemical analyses, and x-ray diffraction.

Exclusive environmental interpretation is not possible, due to the lack of data, and the present knowledge of ancient stromatolites. Thus, several environments are discussed, with preference given to the one most easily fitting the data. The preferred environment is that of a shallow-sloping, tidal platform, with a northeast-southwest trending shoreline. A small regression is followed by gradual subsidence, at the edge of the platform, forming large stromatolitic bioherms.

CHAPTER 1

INTRODUCTION

Location and Access

The study section is located on Kent Peninsula, on a point of land on the northern coast of Parry Bay (see Figure 1). The nearest permanent settlement is an Eskimo community, Baychimo Harbour, 75 km to the south. The nearest town is Cambridge Bay on the southern coast of Victoria Island (see Figure 1). At the time of this study, a semi-permanent fisheries camp and summer camp for one or two Eskimo families was located 3.5 km west of the study section, at the mouth of a river.

The only practical access to Bathurst Inlet is by plane or helicopter. Runways for small aircraft on wheels occur both at Cambridge Bay and at the community of Bathurst Inlet about 165 km south of the study area (Figure 1). The most common access for field parties is by float-equipped Twin Otter. The inlet is usually free of ice during the last part of June and the months of July and August. Transportation in Bathurst Inlet was provided by 6 metre Zodiac boats.

Previous Work

O'Neill (1924) gave the first written account of the geology in the Bathurst Inlet area. He mapped the Epworth Dolomite (Aphebian) which in the present study is the Parry Bay Formation of Helikian age.

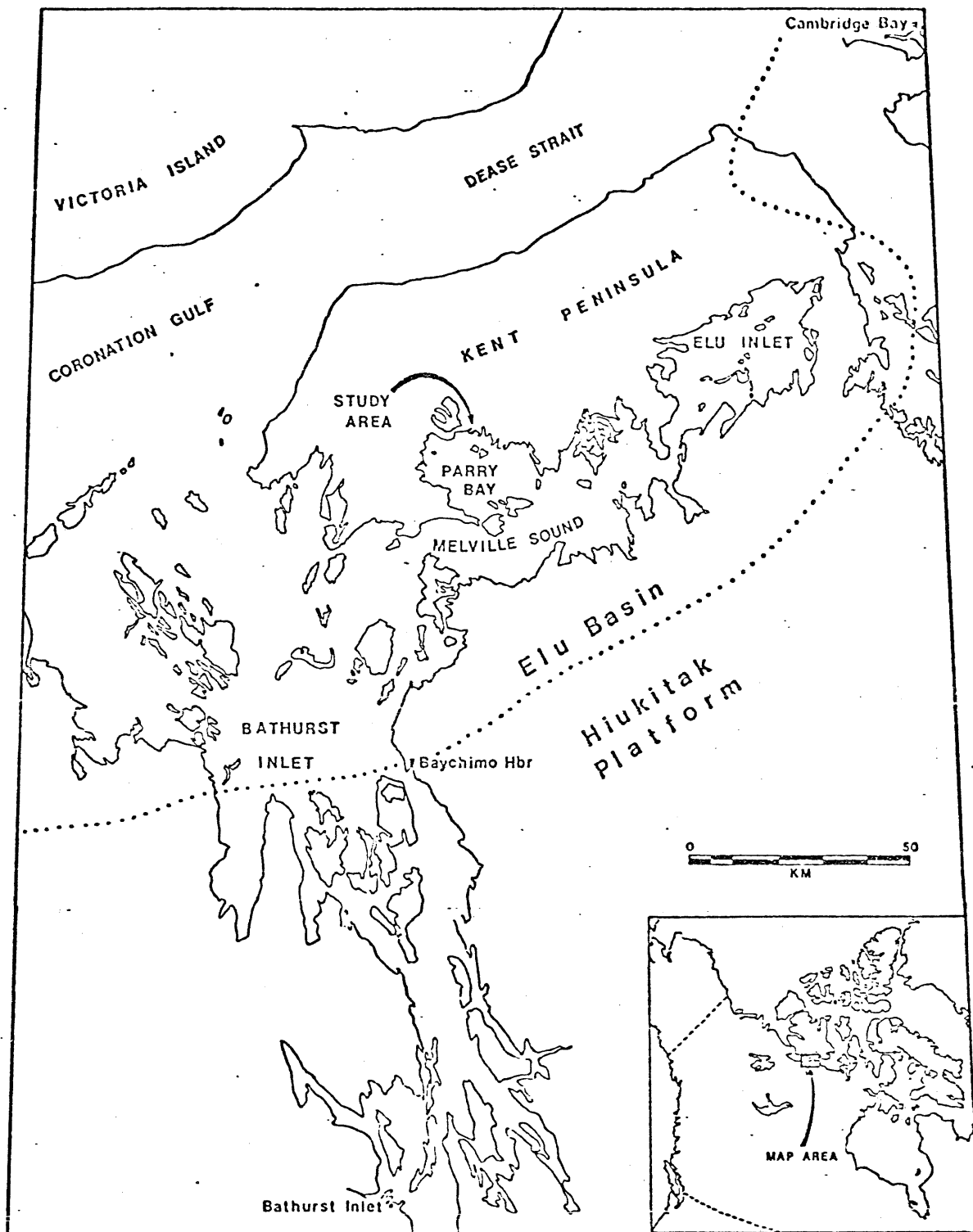


Figure 1. Map showing location of study area. The Elu Basin-Hiukitak Platform boundary is of Helikian age.

J. A. Fraser completed a helicopter reconnaissance survey, including the Bathurst Inlet area, in 1964. The Parry Bay Formation was defined using the northerly trending dolomitic ridges on southwest Kent Peninsula as the type locality.

The first detailed study of the geology of Bathurst Inlet was initiated in 1974, by F.H.A. Campbell of the Geological Survey of Canada, with a study of the Aphebian-aged Goulbourn Group. During the 1977 and 1978 field seasons, the author was involved in the beginning and completion of a detailed study of the Helikian-aged rocks in the Bathurst Inlet area.

Regional Geology

The stratigraphy of Bathurst Inlet is summarized in Table 1 (Campbell, 1979). The geology in the vicinity of the study area is shown on Figure 2.

Aphebian-aged fluvial quartzites of the Burnside River Formation are the only rocks of the Goulbourn Group exposed in the region. Helikian sedimentation began with deposition of the fluvial Tinney Cove Formation, a regolith of which is exposed 30 km to the east of Figure 2. Deposition of the Ellice River Formation began sedimentation on both the Hiukitak Platform and the Elu Basin, and consisted of braided fluvial sediments transitional into a quartz-sand dominated, deltaic complex. Carbonate rocks were deposited geographically beyond

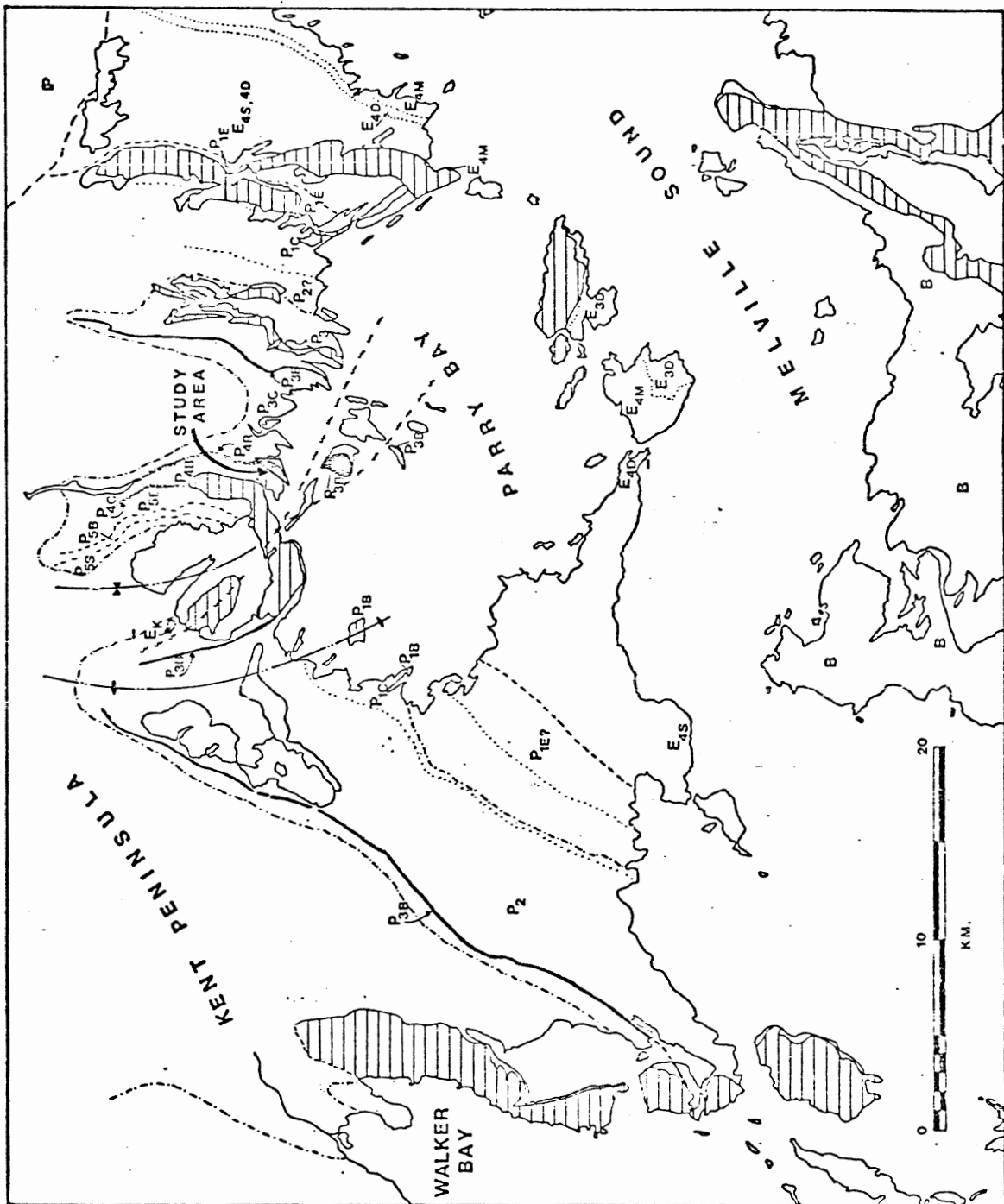


Figure 2. Distribution of the various members of the Parry Bay Formation in the Melville Sound area (adapted from Campbell, 1979). The solid black pattern is the conical stromatolite member (P_{3B}). Other members are as listed in Table 1. The horizontally-stripped areas are diabase sills. The dashed and dotted line represents the approximate limits of outcrop. The dashed line is the southern limit of the Paleozoic cover.

the limits of clastic sedimentation. These rocks comprise the uppermost portion of the Ellice River, as well as the Parry Bay Formation.

The general tectonic setting during deposition of the Parry Bay Formation continues the sedimentary trend begun by the Ellice River Formation; i.e. the Hiukitak Platform to the south and the Elu Basin to the north. The approximate platform edge runs in a northeasterly direction as shown in Figure 1, thus all rocks in the region of the study area were deposited in the Elu Basin.

The youngest Helikian rocks, in the region of Figure 2 are the Ekalulia Basalts. These occur in the centre of a syncline. Hadrynian-aged diabase sills commonly cap dolomite sections and so preserve the strata. Undifferentiated Paleozoic sediments occur immediately to the north of Figure 2.

Purpose of Thesis

The subject of this thesis is a sedimentary section stratigraphically situated in the central portion of the Parry Bay Formation. This section includes the complete P_{4R} member, as well as the upper and lower parts of the immediately underlying P_{3C} and overlying P_{4E} members respectively (Table 1). A more complete section of the P_{3C} member occurs to the west of the study area, in Walker Bay. Unfortunately the Walker Bay section was only mapped during the last day

TABLE 1

Summary of the stratigraphy of the Bathurst Inlet Area
(from Campbell, 1979).

		Diabase sills and dykes		
		Intrusive Contact		
		Jameson Island sediments	Quartzite, quartz-pebble conglomerate, minor siltstone (35 m)	
-----Contact relationships uncertain-----				
MAD-RUNAN	Algak Fm.	A1	Reddish to purple arkose and siltstone; minor mudstone and shale (35 m)	
	Ekalulia Fm.	Ek	Massive olive-green basalt; minor pillowed basalt; rare doloarenite (300-500 m)	
	Kanuyak Fm.	KK	Dolomite block megabreccia; chert-pebble conglomerate; minor quartzite; coarse-grained doloarenite; oolitic and pisolitic dolomite; stromatolitic dolomite; red arkose, siltstone and mudstone (0-60 m)	
-----UNCONFORMITY-----				
H E L I K I A N	P A R R Y B A Y F O R M A T I O N	N A O Y A K R E E F C O M P L E X	P _{5U}	Medium- to fine-grained doloarenite, dolosiltite; stromatolitic dolomite
			P _{5S}	Algal laminated sheets of fine-grained doloarenite, on P _{5C}
			P _{5C}	Bioherms of sheets of laterally-linked low domal stromatolites of fine-grained doloarenite, on P _{5B}
			P _{5B}	Reddish bioherms of sub-vertical laterally-linked poorly-branching columnar stromatolites of fine-grained doloarenite; inter-bioherm channels filled with planar+cross-bedded medium- to coarse-grained doloarenite; on top of P _{5E}
			P _{5E}	Tabular bioherms of narrow, continuous elongate columnar stromatolites of fine-grained doloarenite; minor grey shale
			P _{4C}	Fine- to medium-grained doloarenite; mudstone; red and purple shale and siltstone
			P _{4B}	Reddish bioherms of sub-vertical laterally-linked columnar stromatolites, in sheeted, steep-sided domes; on top of P _{4E}
			P _{4E}	Tabular bioherms of narrow, continuous elongate columnar stromatolites of fine-grained doloarenite; rare isolated stromatolite biscuits near the contact with P _{4R}
			P _{4R}	Red siltstone, mudstone, shale; intraclast-bearing medium-grained and coarse-grained doloarenite; minor domal stromatolite of fine-grained doloarenite
			P _{3C}	Coarse-grained intraclast-bearing doloarenite with rare quartz pebbles; intraformational carbonate-pebble conglomerate; minor stromatolitic dolomite
			P _{3B}	Low-relief bioherms of laterally-linked columnar stromatolites; laterally-linked, large-scale conical stromatolites; black shale and mudstone
			P ₃	Intraclast-bearing coarse-grained doloarenite; carbonate-pebble conglomerate; minor low domal stromatolites
			P ₂	Tabular bioherms of elongate, laterally-linked, low-amplitude domal stromatolites of fine- to medium-grained doloarenite; minor intraclast-bearing doloarenite
			P _{1H}	(Hiukitak Platform facies) Fine- to coarse-grained doloarenite; dolosiltite; rare dololite; minor grey-black shale and mudstone; stromatolitic doloarenite; oolitic, pisolitic dolomite; intraclast-bearing dolomite; rare chert-pebble conglomerate and concretionary dolomite.
			P _{1C}	Medium- to fine-grained doloarenite; low-amplitude domal stromatolite of fine-grained doloarenite; minor grey and black shale and mudstone
P _{1B}	Chaotic megabreccia of angular blocks of P _{1E} and P _{1C} rocks in a matrix of smaller angular fragments			
P _{1E}	Fine- to medium-grained doloarenite; intraclast-bearing doloarenite; isolated small biscuit-type stromatolites; gypsum laminae; salt casts			
E L L I C E R I V E R F O R M A T I O N		E _{4D}	Red, maroon, muddy coarse-grained doloarenite; minor red shale and mudstone	
		E _{4M}	Red and grey shale and mudstone; abundant salt casts; minor quartzite-filled channels and buff fine-grained doloarenite	
		E _{3C}	Medium- to coarse-grained quartzite, planar-cross-bedded; coarse-grained cross-bedded doloarenite; minor stromatolitic dolomite; rare oolitic and pisolitic dolomite; rare mud cracks in red shales	
		E ₃	Planar and rarely trough-cross-bedded coarse-grained white and buff-grey quartzite; minor quartz-pebble conglomerate	
		E ₂	Coarse-grained, large-scale trough-cross-bedded quartzite, grit and quartz-pebble conglomerate; minor siltstone and rare shale; conglomerate in basal parts of fining-upward cycles	
		E _{1B}	Reddish, vesicular, massive basalt (southern Bathurst Inlet area only)	
		E ₁	Very coarse-grained, trough-cross-bedded and massive quartz grit, conglomerate and quartzite; quartzite boulder conglomerate where this unit overlies the Apebian Burnside River Formation	
E _{1R}	Locally-developed, strongly hematitic, saprolitic-weathered regolith; primarily of granitoid Archean rocks (Melville Sound-Elu Inlet area)			
-----UNCONFORMITY-----				
T I N N E Y C O V E F O R M A T I O N		T ₂	Reddish, pink and locally mottled, poorly-sorted arkose and arkosic grit; minor quartz-pebble-bearing arkose and grit and siltstone	
		T ₁	Red, very coarse-grained fanglomerate and quartzite-block megabreccia; coarse-grained polymictic conglomerate	
		-----UNCONFORMITY-----		
D P H E B I A N G O U L B U R N G R O U P		Amagok Formation		
		Brown Sound Formation		
		Kuuvik Formation		
		Peacock Hills Formation		
		Quadyuk Formation		
		urnside River Formation	Red, pink, grey and purple quartzite, quartz grit and conglomerate; ubiquitously trough-cross-bedded; quartz-boulder conglomerate	
		Western River Formation		
-----UNCONFORMITY-----				
A R C H E A N		Undifferentiated gneissic, granitic, metasedimentary and metavolcanic rocks		

of the field season.

A bioherm of low-amplitude, domal stromatolites of the P₂ member occurs stratigraphically below the study section, and is overlain by intraclast-bearing coarse-grained dolarenite of the P₃ member and bioherms of laterally-linked, columnar stromatolites and conical stromatolites. Overlying the study section are a series of large bioherms, 80 m long and 20 m high, composed of elongate, laterally-linked, narrow columnar stromatolites.

The purpose of this thesis was to make an environmental interpretation of the study section. The rock types and field relations within the study section were studied, as well as their relation to the regional stratigraphy. To gain a better understanding of the rock types in the study section and their mineralogy, polished slabs and thin sections were studied, the weight percents of insoluble residue as well as of Ca, Mg, Fe, Mn, Al, CO₂ were determined, and the rocks were stained for calcite. X-ray diffraction was done in order to further aid in mineral determinations, especially of the clay assemblage. Stromatolitic structures played a major role in determination of the ancient environment.

Following a review of the various sources of data and their results, both field and laboratory integration of all the data produced the most plausible environmental interpretation.

Field Methods

The field work for this project was done while working as an assistant for the Geological Survey of Canada at Bathurst Inlet. After mapping two portions of the sections as part of the summer's regional mapping, the author returned to the section to spend three days of sampling and further detailed measuring of the sections.

The thickness of lithologies, as recorded in Figure 3, were measured with a 1.5 metre stick to the nearest 0.1 metre. Locations of measured sections were chosen at the thickest available outcrop at regular intervals (100-300 m) or where there appeared to be any significant change in lithology. Between the measured sections, much of the section is absent or covered by talus, which also limited the length of the measured sections. Sections L, N and O begin at sea level while other sections begin at the lowest outcrop.

While measuring the first sections, samples were taken as representative of each new lithology, and their location in the section recorded. In further sections, located samples of lithologies occurring in previous sections were taken for possible chemical comparison.

Section locations were plotted on a 1:63,360 cm scale air photograph by pacing and using the local topography. Ripple mark and elongation directions were measured with a Brunton compass to the nearest 10 degrees. Strata were essentially horizontal with an average dip of 5°, so no rotation of paleocurrent directions was necessary.

Approximately one-half hour was spent studying the more complete section in Walker Bay. The author was also personally exposed to many of the rocks in the Ellice River and Parry Bay Formations, during the two summers as a field assistant in the Bathurst Inlet area.

Terminology

Stromatolite classification scheme (introduced by Logan et al. (1964))

LLH-S: spaced lateral linkage of hemispheroids

LLH-C: close lateral linkage of hemispheroids

SH: discrete, vertically stacked hemispheroids

SH-V: stacked hemispheroids with variable radius,
upper hemispheroidal laminae do not reach
the base of the preceding laminae

SH-C: stacked hemispheroids with constant
radius

Descriptive Terms added (this paper)

Logan's classification has been adapted for this paper to allow for lateral linkage of stacked hemispheroids.

columnar stromatolites: heights exceed widths greater than 1:1

low (amplitude) domal: widths exceed heights greater than 1:1

sub-circular columnar stromatolites: SH-V with sub-circular plan view
average L:W = 1.5:1

elongate columnar stromatolites: SH-V with elongated plan view
average L:W = 4:1

stroma: short term for stromatolite

doloarenite: clastic, recrystallized dolomite, grains of sand-size

dolosiltite: very fine-grained, green, clastic, recrystallized, dolomite
grains of sand-size

mudstone: red coloured fine-grained calcareous sediment

shale: calcareous shale, red or green .

ACKNOWLEDGEMENTS

I wish to thank Dr. F.H.A. Campbell for his supervision, encouragement, helpful suggestions and many enlightening discussions during the field season without which this thesis would not have been possible. The Geological Survey of Canada financed much of this project, including field work, drafting supplies, and photographic reductions of the fence diagram. Thanks are extended to Dr. P. E. Schenk for critically reading the manuscript and offering useful suggestions for its improvement. G. McIsaac assisted with field work. The geochemical portion of this study was supervised by S. Parikh. Dr. H.B.S. Cooke, Dr. W. Ervine, and Dr. G. C. Milligan are gratefully acknowledged for their assistance and suggestions at various stages in the thesis work. I would also like to thank G. Davison and R. Sproule who ran samples for x-ray diffraction, and S. Harnish for printing the photographs of the hand samples.

CHAPTER 2

FIELD DESCRIPTION OF UNITS

The study section can be divided into eight informal units based on a combination of lithological character and the presence or absence of stromatolites. These units can be traced along the entire study section, as well as into the Walker Bay section. The fence diagram (Figure 3, located in Figure 4) shows the vertical succession of the various lithosomes and their lithic correlation. Figures 5 and 6 are composite schematic cross-sections of units $3C_1$ to $4R_3$ and $4R_4$ respectively. Unit $4R_4$ has been further subdivided on the basis of variation in stromatolite morphology.

The following is a description of each unit together with its relation to other units. Where possible, data from the Walker Bay section is combined with that of the study section for interpretive purposes.

Unit $3C_1$

Unit $3C_1$, which occurs only in section L (Figure 3), is a coarse-grained dolarenite at least 1.4 metres thick (measured from its lowest exposure at sea level). It is medium bedded and weathers to a clean, white, massive dolomite with widely spaced, low-domal stromatolites of similar composition. These stromatolites range in

Figure 3. Fence diagram of the study section (located in Figure 4), showing the vertical succession of the various lithosomes and their lithic correlation.

The diagram has been drawn such that the top of unit 4R₃ is horizontal. The remaining portions of each section have been positioned relative to that plane. Measured sections are labelled A to O, and the top of unit 4R₃ is positioned at the cross, but projected vertically downwards from this horizontal plane.

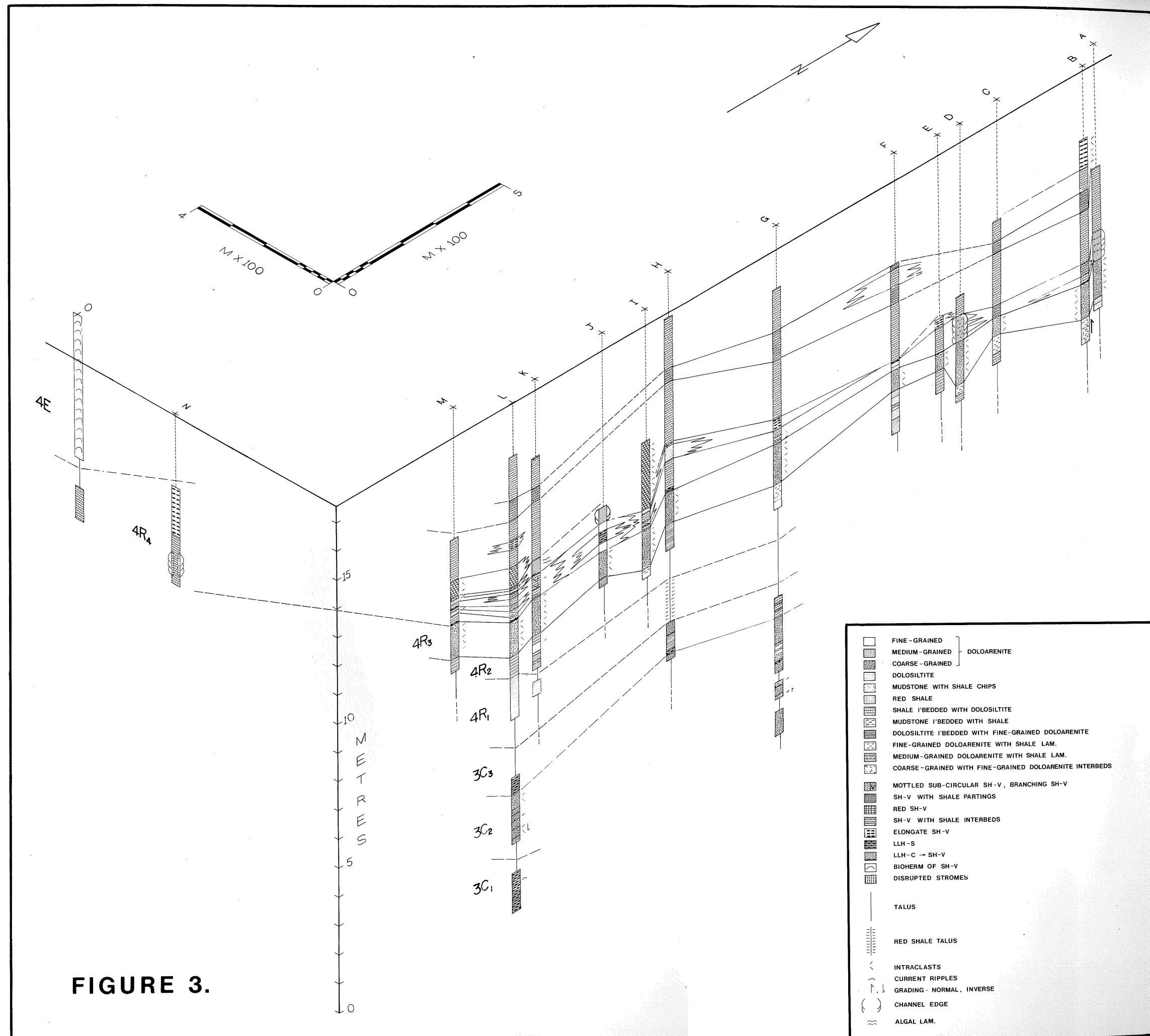


FIGURE 3.

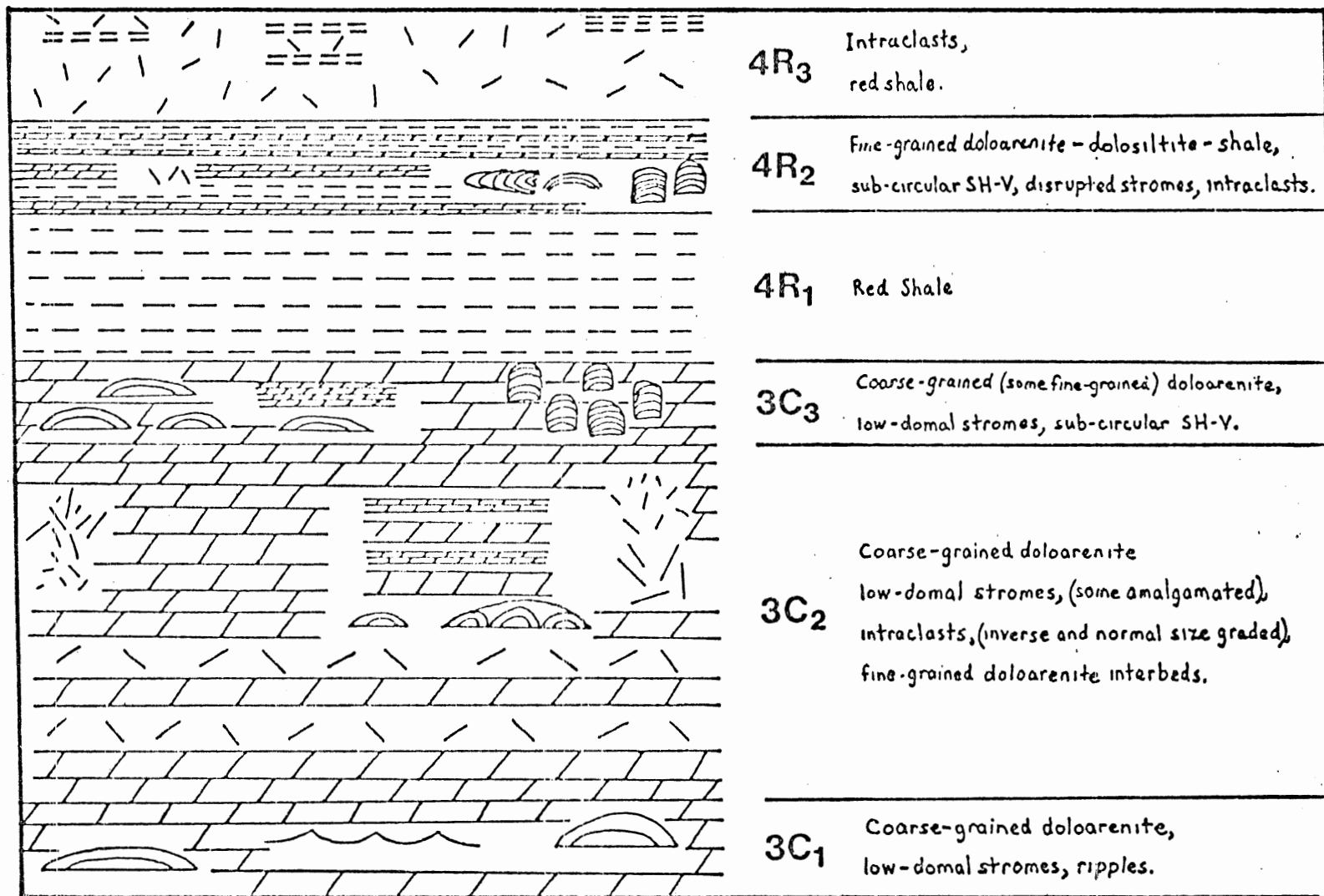


Figure 5. Composite schematic cross-section of Units 3C₁ to 4R₃.

length from 15-60 cm and have an average relief of about 5-10 cm (see Plate 1). Some are slightly elongated in northwest-southeast directions (L:W = 1.4:1). In the Walker Bay section, low domal stromatolites of this unit are larger with reliefs of about 1 metre. Straight symmetrical ripples with the long axis of their crests oriented at 025° and 45° are also present.

Unit 3C₂ Coarse-grained doloarenite

Unit 3C₂ varies in thickness from 2.7 metres in section L to over 4.1 metres in section G (see Figure 3). Finely laminated, massive weathering and thin to medium-bedded coarse-grained doloarenite beds alternate with .1-.5 metre thick intraclastic beds. A thin stromatolite layer occurs in section G.

Normal or inverse size-grading of intraclasts occurs in some intraclastic beds (see Figure 3). Normal grading begins with finely laminated, elongated laths (average 2.5 cm in length) lying parallel to the bedding. These grade upwards into smaller (average 3 by 1 mm), finely laminated, almost elliptical-shaped intraclasts which are randomly oriented. Some larger intraclasts occur dispersed among the smaller intraclasts. Inverse grading begins with small, round to lath-shaped intraclasts resting irregularly on greenish-grey lime mud. These grade upwards into larger, long, thin, finely laminated intraclasts (20 by 1 mm) which lie at oblique angles to the bedding.



Plate 1. Plan view of a low-domal stromatolite in unit $3C_1$. Scale is a Brunton compass.

Widely spaced, low-domal stromatolites form the upper surface of a coarse-grained doloarenite bed in section G (see Figure 3). These are small (10 cm diameter) and may be slightly elongated. Some have amalgamated to form larger elongate stromatolites (34 by 27 cm). The stromatolites are overlain by coarse-grained medium-bedded doloarenite with interlayers of fine-grained doloarenite (see Figure 3).

The contact of unit $3C_2$ with unit $3C_3$ is indistinct. The base of unit $3C_3$ is marked by the reappearance of stromatolite beds.

Unit $3C_3$

Unit $3C_3$ averages 1.1 metres thick, and is defined by a basal stromatolite stratum and capping shale strata. Lithic correlation is very difficult in this unit because of poor outcrop exposure and the lateral discontinuity of lithologies (see Figure 3).

Coarse to medium-grained, low-domal stromatolites (30 cm diameter) at the bottom of the unit in sections H and L (see Figure 3) have either light and dark green, or light green and red, undulating, convex laminations. Cross-laminations may cut previous laminations on the flanks of the stromatolites (sample L5, see Appendix 1).

Lateral to the domal stromatolites is a 70 cm thick stratum of coarse-grained doloarenite with mottled, sub-circular, columnar stromatolites (10 cm in diameter). Stromatolite laminations are

irregular, and alternations of green and red laminae end abruptly at the wall of the stromatolite (sample G6, Appendix 1). Inter-stromatolitic material is coarser-grained and massive, with red and green mottles. Stromatolites, of this unit, in the Walker Bay section are very elongate, laterally-linked hemispheres with pointed tops.

Reddish-brown, coarse-grained doloarenite overlies thin-bedded, fine-grained doloarenite with undulatory laminations of dolosiltite (see Figure 3). Continuous flat laminations are inter-laminated with thin (.1-1 mm) lenses of clear, colourless dolomite. In places, the laminations are disturbed (see Appendix 1, sample H3 for further description). 1 mm wide ridges, approximately 1 mm in relief, 25 mm in length and spaced 16-21 mm apart, occur on the bedding surface (see Plate 2). When examined closely, two other sets of ridges can be seen superimposed on the main set. One of these sets has ridges 9 mm wide and spaced 12 mm apart, whereas the other set has rare ridges 2 mm wide. These may be micro-interference ripples.

Unit 3C₃ is overlain by shale. The actual contact is not visible due to talus cover; however, the reddish-brown coarse-grained doloarenite is overlain by red shale talus (Figure 3), which is obviously almost in its position of deposition.

Unit 4R₁ Red Shale

Distinctive strata of parallel laminated to thin-bedded, highly



Plate 2. Ridges on the bedding surface of reddish-brown, coarse-grained dolarenites, Unit 3C₃. The orientations of the three sets of ridges are shown with dashed lines.

friable, red shale comprise this unit which is at least 1.5 metres thick, and occurs either as outcrop, or as a fragmented, red shale talus, obviously not far from its original position. A similar unit is also found in the Walker Bay section. Subcircular shallow cracks were found on the bedding surface of the shales in the Walker Bay section.

The contact, between unit $4R_1$ and the overlying Unit $4R_2$ is a transition from totally shale strata to dolosiltite interlayered with shale. The base of unit $4R_2$ is defined by the first dolosiltite layer.

Unit $4R_2$ Mudstone-Dolosiltite Strata

Unit $4R_2$ is a continuous unit (thicker than 1.4 metres) consisting of green, fine-grained doloarenite and dolosiltite, interbedded with red mudstone and shale. Bedding is parallel, with individual beds ranging from laminations to medium bedded. Some mudstones show normal grading on a scale of a few centimetres. Basal, massive, fine mudstone grades up into cross-laminated sediment, which grades upwards into massive, finer mudstone (Section B, Figure 3).

Isolated lenses of red and green laminated, fine-grained, sub-circular columnar stromatolites (10 cm average diameter) occur in the northern portion of the section (see Figure 3). Directly to the left

of the portion of the convex bed shown in Plate 3, where laminations are convex upwards, laminations appear to be those of the average columnar stromatolite in the study section, but are convex horizontally, rather than vertically (Plate 4). Further to the south, in section K, some intraclasts are present in fine-grained doloarenite.

The fine-grained sediment of unit $4R_2$ is abruptly overlain by coarse-grained intraclastic doloarenite of unit $4R_3$. The pronounced difference in weathering resistance of the two units produces a distinctive contact.

Unit $4R_3$ Intraclastic Strata

Unit $4R_3$ forms a distinctive lithic marker-zone of fairly constant thickness (approximately 1.3 metres average). Figure 3 has been drawn such that the top surface of this intraclastic bed is horizontal. Plate 5 suggests the distinctiveness of this unit even at a distance, and Plate 6 shows its relation to underlying and overlying rocks.

The weathered surfaces of the strata are greyish-white and massive to medium-bedded. Red shaley laminations commonly occur interlayered with the intraclastic layers in the upper 20-40 cm of the bed.

The fresh surface is mottled red and green. Intraclasts may be either colour but the matrix is always distinguishable from the

Plate 3. Stratum with convex-upwards laminations, underlain and overlain by shale, unit 4R₂ section F.

Plate 4. Horizontally-oriented, columnar stromatolite located immediately to the left of laminations in Plate 3.



Plate 3



Plate 4

Plate 5. Unit 4R₃ (outlined by dashed lines). Note the distinctiveness of the strata, even at a distance. Scale is a 1 1/2 metre stick. Small divisions are 10 cm.

Plate 6. Unit 4R₃ (outlined by dashed lines), underlain by shale, interbedded with fine-grained dolarenite, and overlain by sub-circular SH-V. The mound-like unit on top is composed of SH-V. The gulley is probably glacial. Scale is a 1 1/2 metre stick.

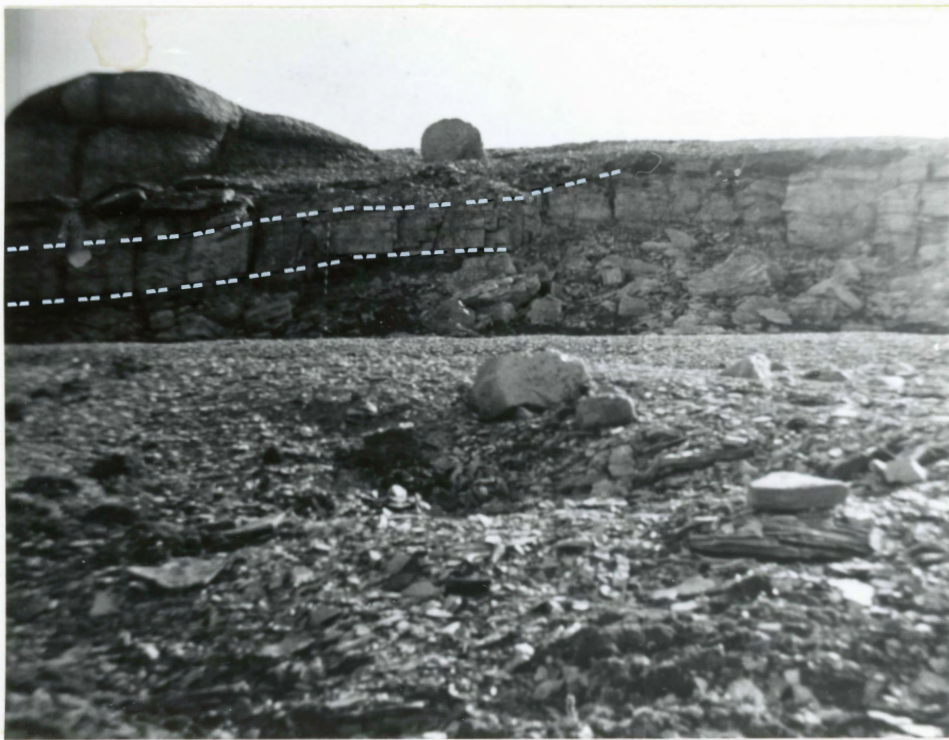


Plate 5



Plate 6

intraclasts by a colour difference. Intraclasts range in size from 40 by 2 cm, to .13 by .03 mm. Larger intraclasts are long and narrow, while smaller ones are either more lath-shaped or sub-circular. Most intraclasts have been rounded. The grain size of intraclasts is similar to that of the matrix, with the exception of coarser cavity-filling dolomite. Plate 7 shows a closeup of the intraclasts in outcrop. Intraclasts can be parallel to the bedding (bottom of the photo) or randomly oriented (farther up in the photo).

In the Walker Bay section, 20-30 cm thick, normally size-graded cycles occur. Intraclasts grade upward into fine-grained doloarenite and into shale. This cycle is repeated several times.

The contact of unit $4R_3$ with $4R_4$, is generally gradational. The upper portion of the intraclastic unit often has laminations of finer material, which gradually increase in thickness to become unit $4R_4$. The top of unit $4R_3$ is here defined as the last bed of coarse-grained doloarenite containing intraclasts, before the appearance of columnar stromatolites.

Unit $4R_4$

Unit $4R_4$ is basically a stromatolitic complex composed of a variety of stromatolite types. There is little continuity of rock or stromatolite type, either vertically or laterally (see Figure 3).



Plate 7. Close-up of an intraclastic stratum, unit 4R₃. Note that intraclasts near the base of the stratum lie sub-parallel to the bedding, whereas farther up in the strata, intraclasts are randomly oriented. Scale is a wooden match stick, approximately 5 cm long.

Thus, beginning at the base of the unit, the various stromatolite types and non-stromatolitic rocks will be described along with their relation to other stromatolite types or rocks. Table 2 shows a diagram of the various types of stromatolites, and lists their dimensions along with their degree and direction of elongation. Figure 6 shows a schematic cross-section of the unit.

Base of Stromatolitic Complex

Sharply overlying the intraclastic doloarenite of unit $4R_3$ is medium-grained, slightly undulating, doloarenite strata. Within 19 cm, strata have become gently convex upwards, to form green and red weathering, low-domal, linked stromatolites. These are approximately 11 cm high, 9 cm in breadth and have a relief of 1.7 cm. Laminations average about 2.6 mm in thickness (see Plate 8). Other basal stromatolites are linked with wavy undulations at their base, but expand upwards to form a dome-shape on top (Plate 9).





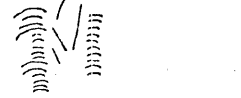

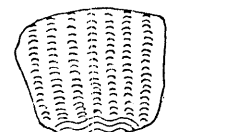
These domal stromatolites occur in isolated patches surrounded by fine-grained doloarenite and shale. They generally grade upwards into sub-circular columnar stromatolites.

Sub-circular SH-V

Sub-circular columnar stromatolites occur in almost massive appearing, red and green mottled sections ranging in thickness from

TABLE 2

Dimensions of stromatolites in Unit 4R₄

Stromatolite	Height (cm)	Synoptic Relief (cm)	Diameter (cm)	Length (cm)	Spacing (cm)	Degree of Elongation (L:W) ratio	Direction of Elongation
EASAL STR S 	11	1.7	9	-	-	-	-
SH-V 	8 - 10 up to 20	3 - 6 when linked 10 when unlinked	8 - 12 average up to 20	average 12	5-10	7:1, 3:1, 1:1	northwest southeast
ELONGATE SH-V 	13 - 23 up to 60	average 3-4 .5 when strong lateral linkage also 1.6 to 6	2 - 5	10 - 56	breadth wise 6 - 9 length wise 4 - 5	17:1 - 2:1 average 4:1	northwest southeast
SH-V with SHALE PARTINGS 	8 - 10 + 20	-	8 - 12	-	5 - 10	-	-
RED SH-V 	8 - 23	8 - 23	variable 2 - 18	-	5 - 6	1:1	
BRANCHING SH-V 	>30	23	19 8 + 2		1.7 - 5.2 increasing upwards	2:1	northwest southeast
ISOLATED STROME MOUND 	250	250 internal columns 1	300 internal columns 3 - 5				

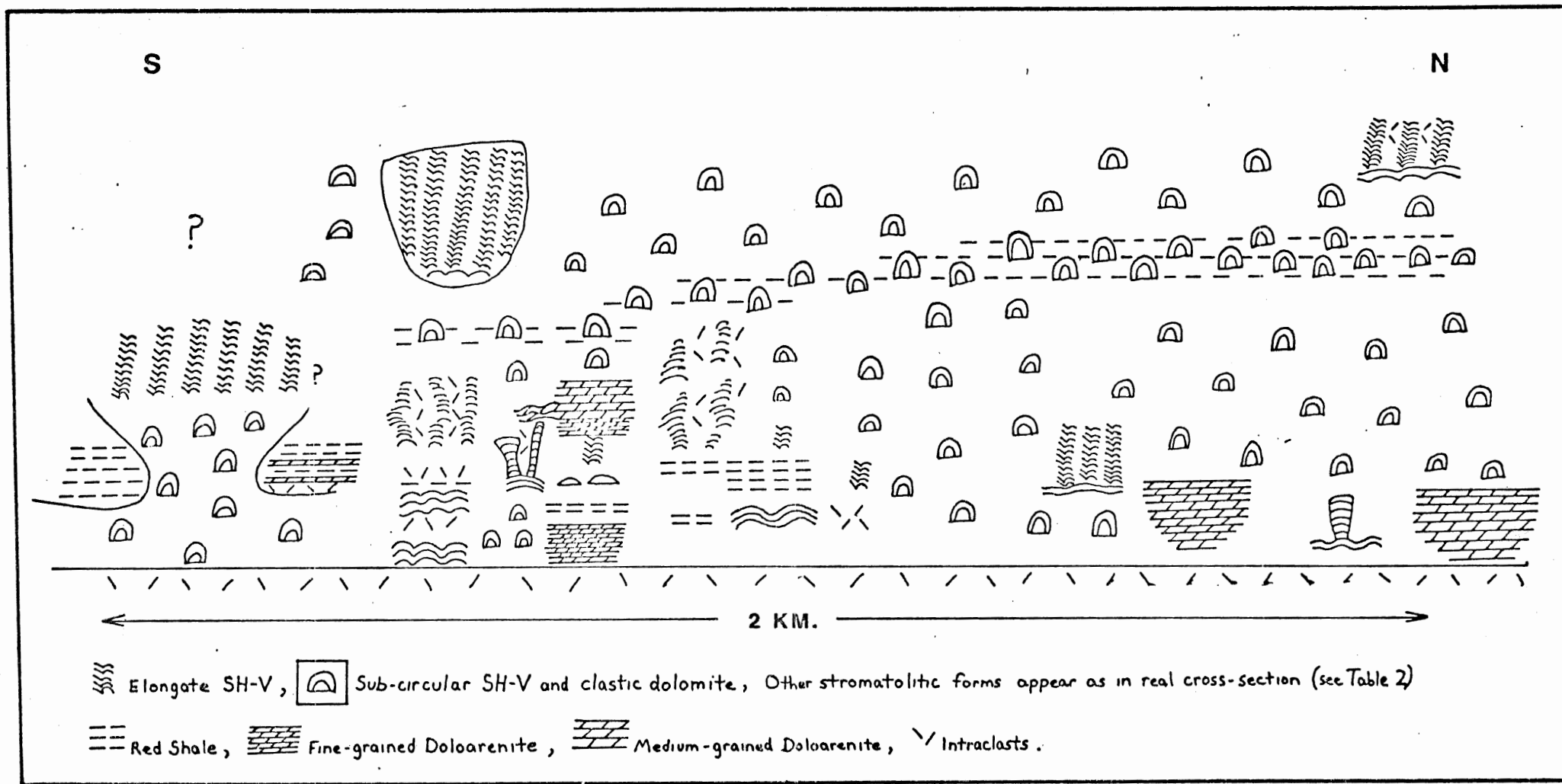


Figure 6. Composite schematic cross-section of Unit 4R₄.



Plate 8



Plate 9

.2 m up to 2.1 metres and comprising the majority of unit 4R₄ (see Figure 3). Laminations of stromatolites can generally only be seen upon close examination of the outcrop in cross-section or by slabbing the rock. Bedding plane surfaces are usually weathered to expose a series of sub-circular shaped domes protruding above the inter-stromatolite sediment (Plate 10). Stromatolites in the lower, southern portion of the section (Section N, Figure 3) appear to have a central core, with a diameter of 1 cm and inner concentric laminations (see Plates 11 and 12).

There are three major intervals of these sub-circular columnar stromatolites. The first interval (average 20 cm in thickness) most commonly branches out from the linked low-domal stromatolites described previously. This interval is overlain by thin-bedded fine-grained dolarenite, mudstone, or shale. In one location (Figure 3) it is transitionally overlain by elongate stromatolites.

The second interval is underlain by red columnar stromatolites (described later), elongate stromatolites (described later), or more generally, by thin-bedded medium-grained dolarenite. Sub-circular columnar stroms are overlain in section N by elongate stromatolites with a sharp distinct contact (see Plate 14).

The third interval is separated from the second, by a continuous layer of columnar stromatolites with shale partings (described later). This interval, in most sections, is overlain by talus; however, section B has a unit of elongate columnar stromatolites overlying the sub-rounded ones (Figure 3).

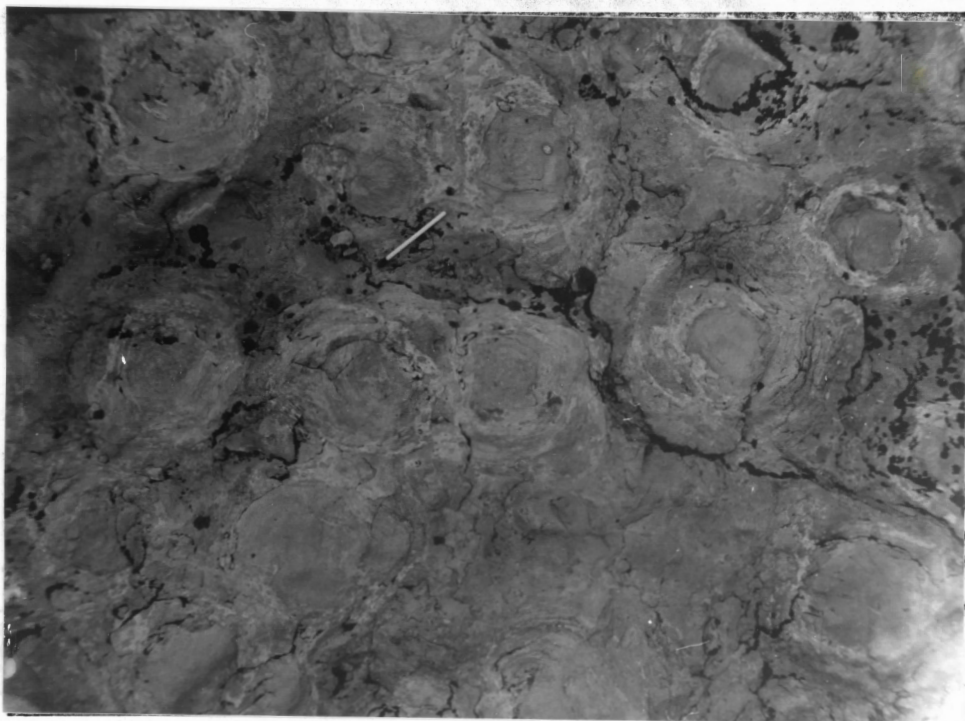


Plate 10. Plan view of sub-circular columnar stromatolites, appearing as small domes protruding above the inter-stromatolite sediment. The wooden match stick is approximately 5 cm long.

Plate 11. Sub-circular columnar stromatolite with a central core.
Horizontal cross-section of the core occurs to the right
of the match stick head.

Plate 12. A vertical cross-section of the central core of a sub-
circular columnar stromatolite is shown just left of
the foot of the match stick.



Plate 11



Plate 12

Plate 13. Plan view of very elongate columnar stromatolites. Stromatolites are the darker ridges. Brunton compass for scale.

Plate 14. Cross-section of elongate columnar stromatolites. Stromatolites are a dark red colour with cracks along their laminations. Note the contact with the underlying sub-circular columnar stromatolites in the lower half of the picture. Wooden match stick (about 5 cm long) for scale, on lower right hand side.

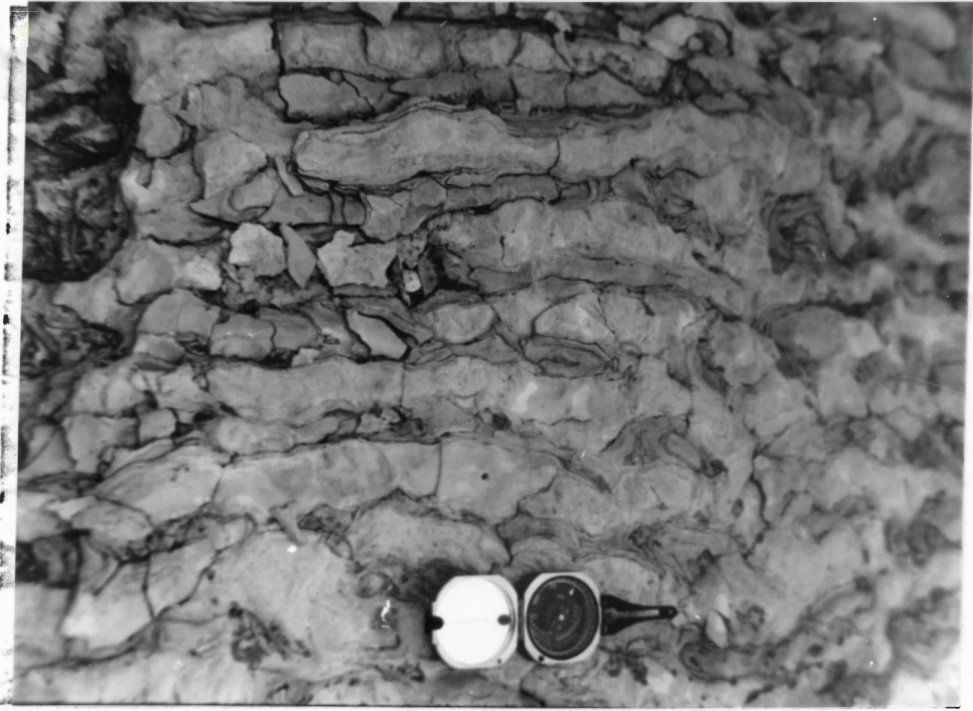


Plate 13



Plate 14

Elongate SH-V

These are pseudo-columnar stromatolites, strongly elongated in plan view, such that they appear as narrow, slightly sinuous, parallel ridges on the bedding plane (Plate 13). In cross-section, the columns are usually quite distinct with cracks along their laminations, and often a darker red colour than the inter-stromatolite material (Plate 14 and 15) (see Table 2 for stromatolite dimensions and elongation directions). This member varies in thickness from 1.7 m to only .1 m and occurs in lenses. It may be continuous along the top of the section but because of talus, it is only exposed in section B.

Inter-stromatolite material is of similar composition to the stromatolites, but is much lighter in colour. Abundant laminations, linking stromatolites, divide the inter-stromatolite material into blocky, lense-shape chunks of intraclastic dolarenite. Larger intraclasts occur between columns where linkage is not present, as in the upper portion of the elongate columns in section B (Figure 3). Intraclasts between columns in section N, are 12 cm long and 1 to 2 cm wide. These intraclasts have a vertical dimension as well as horizontal ones, but a cross-section of the stromatolites at this location was not available. Similar intraclasts in section M (Figure 3), oriented sub-vertically between columns, were 1.5 - 5.5 cm long (Plate 17). These intraclasts were probably thin plates.

Some of these stromatolites have grown at angles of 15 to 28° from the vertical (see Plate 16). The vertical has been assumed to be 90°

Plate 15. Cross-section of elongate columnar stromatolites. Stromatolites are similar in colour to the surrounding sediment but are visible due to cracks along their laminations. Intraclasts occur between columns. Wooden match stick, about 5 cm long, is scale.

Plate 16. Elongate pseudo-columnar stromatolites, growing at angles of 15-28° from the vertical. Stromatolites are distinctive with their dark red colour. Match stick, for scale, is to the right of the middle of the farthest right column.

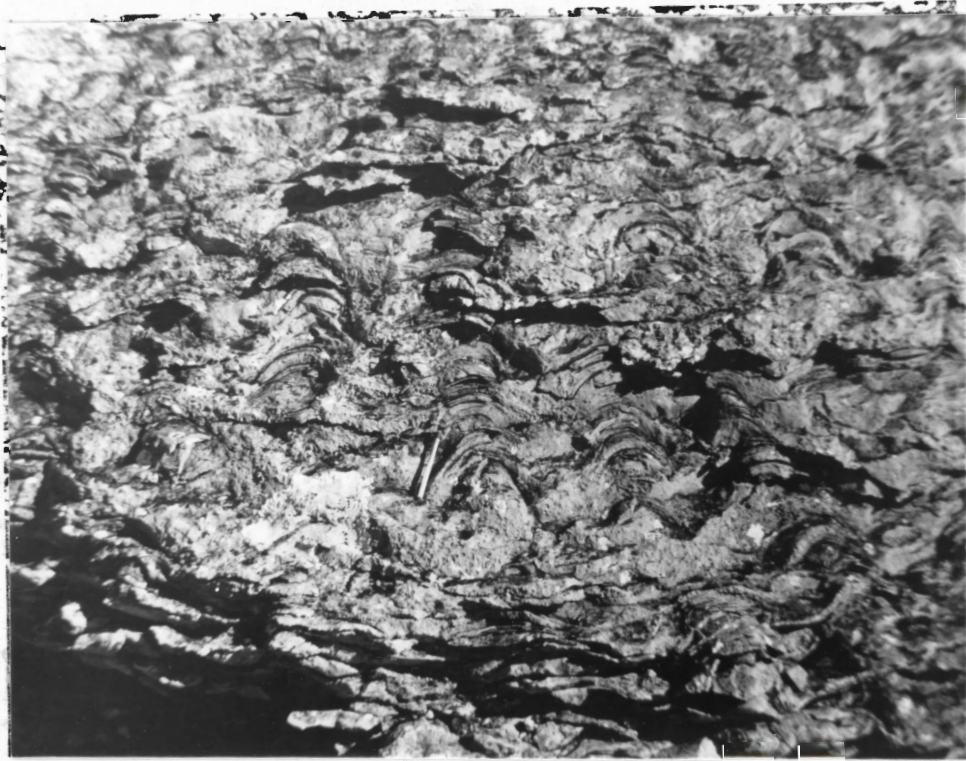


Plate 15



Plate 16

from the linked, slightly wavy laminations from which these columns evolved. The columns have a sinuous upward growth.

These elongate, columnar stromatolites usually overlie and underlie the sub-circular, columnar stromatolites and occur as lenses pinching out laterally. Contacts with the circular stromatolites are gradational, especially the lower contact. In some places, the sub-circular stromatolites may evolve into wavy laminations which then evolve into less strongly linked elongate columnar stromatolites. In section J, (Figure 3), low-domal stromatolites evolve into elongate columnar stromatolites, and in section H, elongate stromatolites overlie a shale unit.

SH-V with shale partings

These stromatolites form a distinctive, continuous zone (approximately 0.7 metres thick) within sub-circular columnar stromatolitic strata. The zone is distinctive in being thin-bedded and red weathering, in comparison to the massive, green weathering sub-rounded stromatolites. The thin-bedding is caused by shale laminations. The actual stromatolites are similar to the sub-rounded ones (see Table 2).

The contact with the massive green weathering stromatolites is gradational over a few centimetres.

Red SH-V

These columnar stromatolites are clearly visible because of the contrast of their red and green laminations against the massive green dolarenite between the stromatolites. Their diameters increase or decrease irregularly upwards, giving the appearance of sinuous upward growth. No lateral linkage occurs between stromatolites and the plan view is sub-rounded (see Table 2 for dimensions).

Intraclasts occur between columns in section M and I but not L (Figure 3). Intraclasts between columns in section M are long and narrow (1.5-5.5 cm long by 1-2 mm wide) and are oriented sub-vertically between the stromatolites (see Plate 17). As discussed earlier with respect to the elongate columnar stromatolites, these are probably thin plates. The upper portion of the stromatolite is similar to a domal head, larger than the lower portion of the stromatolite. Layers may have peeled off this and been preserved as sub-vertical intraclasts.

The red columnar stromatolites are underlain by intraclastic, coarse-grained dolarenite or by shale and are overlain by sub-circular columnar stromatolites. Laterally the red columnar stromatolites pinch out, grade into the sub-circular columnar stromatolites or are cut by medium-grained dolarenite (see Figure 3).

Branching SH-V

An isolated occurrence of a branching stromatolite was found in



Plate 17. Subvertical intraclasts between red SH-V (section M). Match stick for scale is about 5 cm long, in lower left corner.

a 50 cm thick unit in section K (see Figure 3). The stromatolite began as dome-shaped, with a diameter of approximately 19 cm and branched into two arms (8 cm diameter decreasing to 5 cm and 2 cm diameter) angling away from each other (see Plate 18). Stromatolite laminations are dome-shaped and are visible by their dark red colour. Intraclasts occur between the two branches.

The branching stromatolites grade up from a bed in which stromatolites are just beginning to form, and are overlain by an algal-laminated, medium-grained doloarenite. Laterally they either gradually become the normal sub-circular columnar stromatolites or are replaced by fine-grained doloarenite.

Isolated Stromatolitic Mound

A large stromatolitic mound (approximately 2.5 m high and less than 3 m wide) occurs near the top of the section (not shown in Figure 3). This mound consists of narrow (2-3 cm diameter) columns of vertical stromatolites. Some of these have evolved from linked, low-domal stromatolites (see Plate 19) (also see Table 2 for dimensions of the stromatolites).

Stylolites occur 1/3 and 2/3 up in the mound and cut horizontally across the mound. Above the upper stylolite, stromatolites are abruptly smaller (2.3 cm diameter rather than 3-5 cm) and more widely spaced. The relief remains the same.

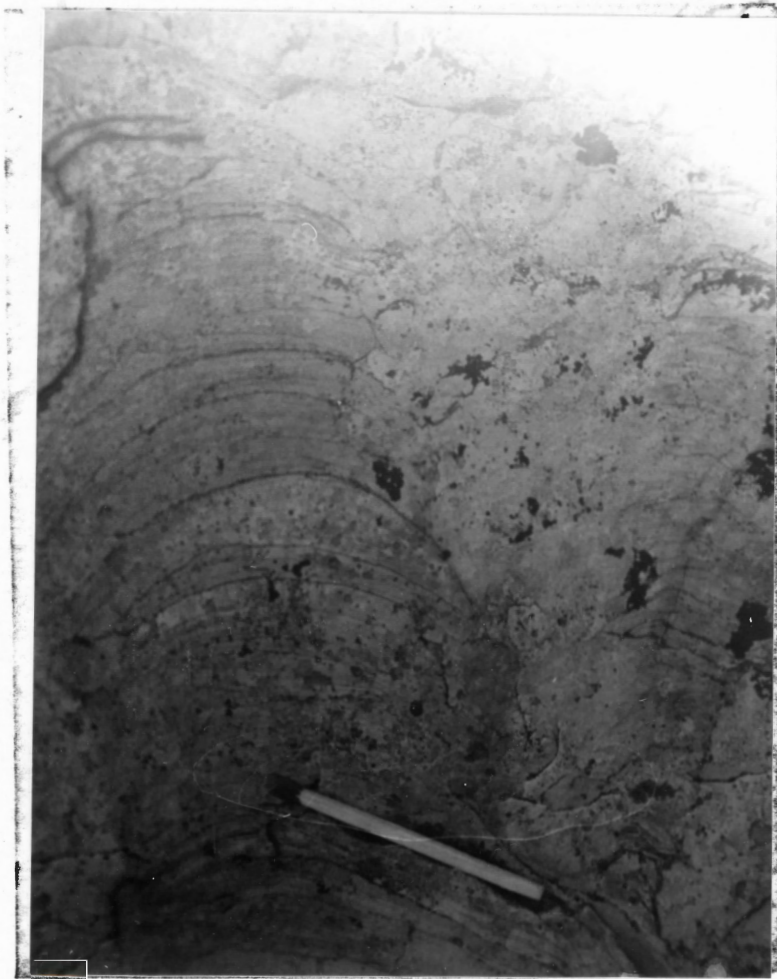


Plate 18. Dark red, branching SH-V with a large branch to the left and a smaller branch to the right. Intraclasts occur between branches. Wooden match stick, about 5 cm long, for scale.

Plate 19. Low-domal, close-linked stromatolites evolving into narrow, vertical, pseudo-columnar stromatolites (Brunton compass for scale in lower left corner).

Plate 20. Channel deposit in section N, showing beds pinching out and dipping towards the mound of sub-circular and elongate columnar stromatolites to the left. Dark shale exposures occur in patches at the top of the deposits. Note: The negative was printed inversed such that the mounds at the left should be to the right.

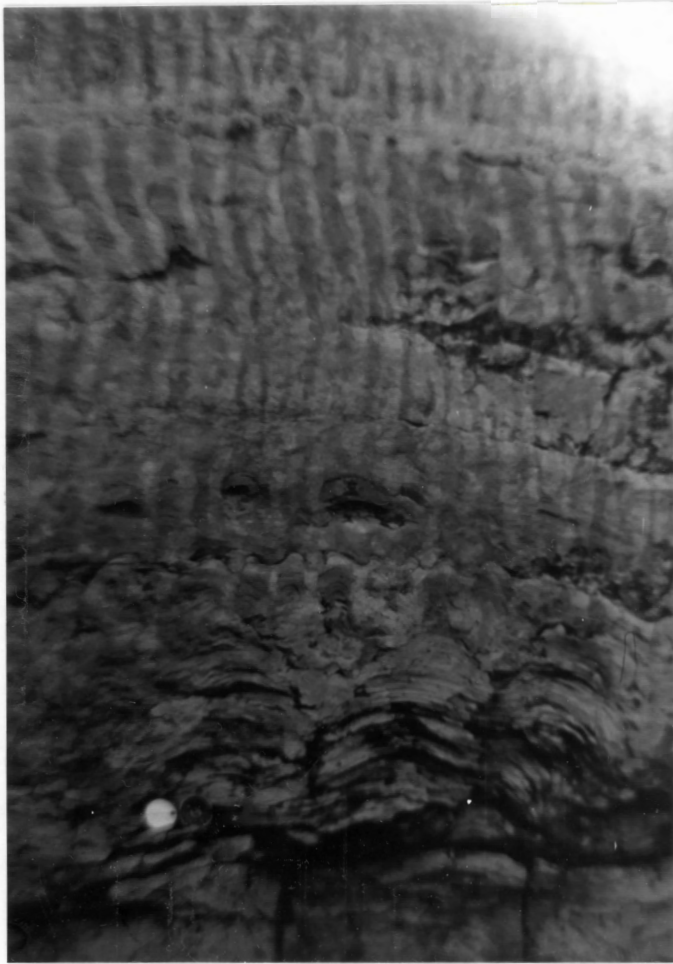


Plate 19

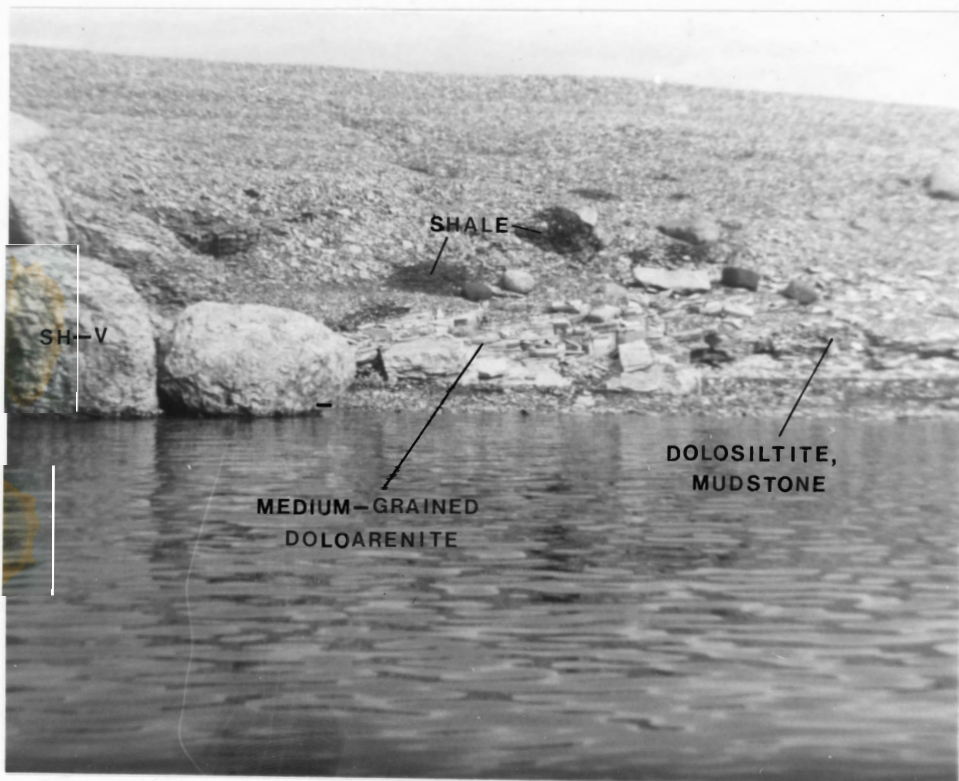


Plate 20

The low domal stromatolites at the bottom of the mound are 4.6 cm high and 40 cm in diameter. The form either decreases in diameter gradually upwards, until it is the diameter of the thin columnar stromatolites, or it branches into two of the narrow columns.

This large mound is underlain sharply by massive, coarse-grained doloarenite and overlain by talus. It is an isolated mound with sharp contacts between the massive sub-circular columnar stromatolites and clastic doloarenite.

Channel Deposits

A number of small channel deposits occur in the lower portion of unit 4R₄, and at least two more major channels are in sections J and N (see Figure 3).

In section N, the base of the channel consists of a green intra-clastic doloarenite bed, overlain by interlayered shale, mudstone and dolosiltite grading up into parallel, thin-bedded, green, medium-grained doloarenite. Laminated red shale and mudstone lie on top (see Plates 20 and 21, and Appendix 1). The channel deposit is sharply underlain by a massive unit of sub-circular columnar stromatolites, and dips towards and pinches out into a 3.5 m high mound of sub-circular and elongate, columnar stromatolites (Plate 20). A total thickness of 1.5 m is exposed, and extends laterally for about 12 m.

In section J, (Figure 3) thin-bedded to laminated red mudstone

Plate 21. Channel deposit from section N. Sub-circular columnar stromes are sharply overlain by intraclastic doloarenites. Shale, mudstone and dolosiltite grade up into the shale (1.5 metre stick for scale).

Plate 22. Thin-bedded to laminated, red mudstone and fine-grained, green doloarenite are sharply overlain by very flat parallel beds of medium-grained doloarenite (section J, Unit 4R₄) (1.5 metre stick for scale).



Plate 21

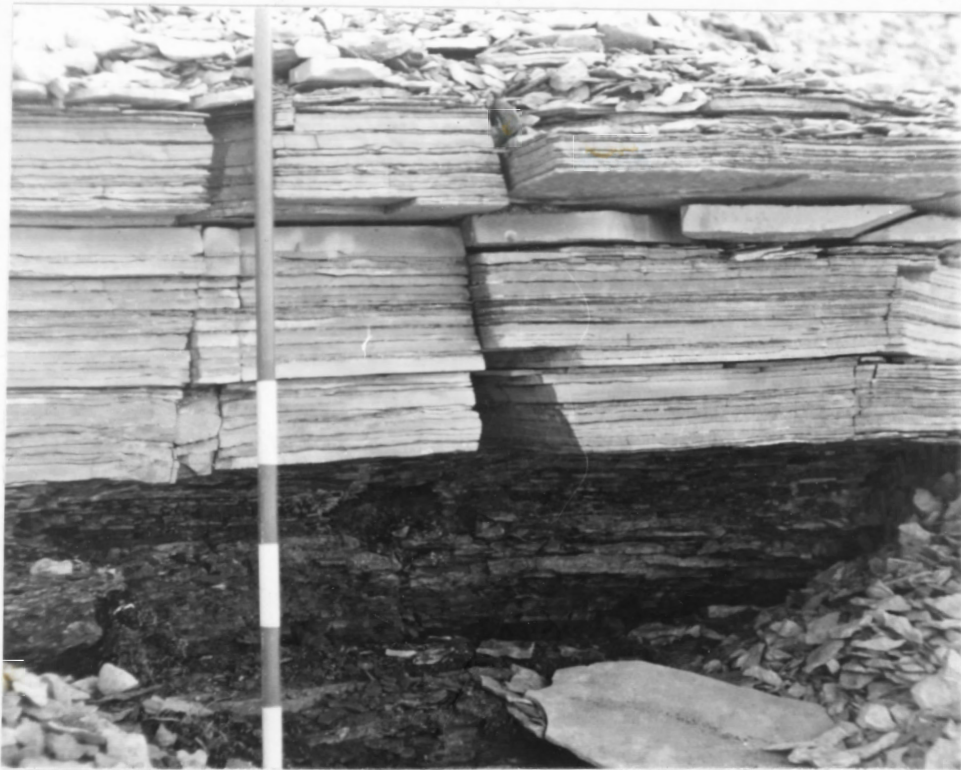


Plate 22

and fine-grained, green doloarenite are overlain with a sharp flat contact by very flat parallel beds of medium-grained doloarenite. Beds range in thickness from 2-4 cm (see Plate 22).

Less distinct channels between stromatolite mounds commonly occur directly above the intraclastic unit $4R_3$. The more prominent of these channels are composed of medium-grained, flaggy doloarenite with red shale laminations. A number of thin lenses of coarse-grained doloarenite, fine-grained doloarenite, or mudstone and shale also occur throughout the lower portion of the unit. Shale strata in section H have sub-circular cracks on the bedding surface. Internal semi-radial cracks occur within each circular crack (Plate 23).

Unit 4E Bioherms

Bioherms (at least 6 m high and 12-15 m wide) (Plate 24) lie on top of the stromatolites of unit $4R_4$. The lower portion of the one bioherm examined is composed of strongly elongate linked columns with intraclasts between columns. Columns are of various sizes and have variable diameters. Some small oval-shaped stromatolites (no more than 3 cm in diameter) occur in isolated patches.

The upper portion of the bioherm consists of very strongly elongate (Plate 25) narrow stromatolitic pseudo-columns with diameters of 3-4 cm and heights of greater than 25 cm. SH-V with shale partings are shown in the lower part of Plate 26 grading up to the more massive

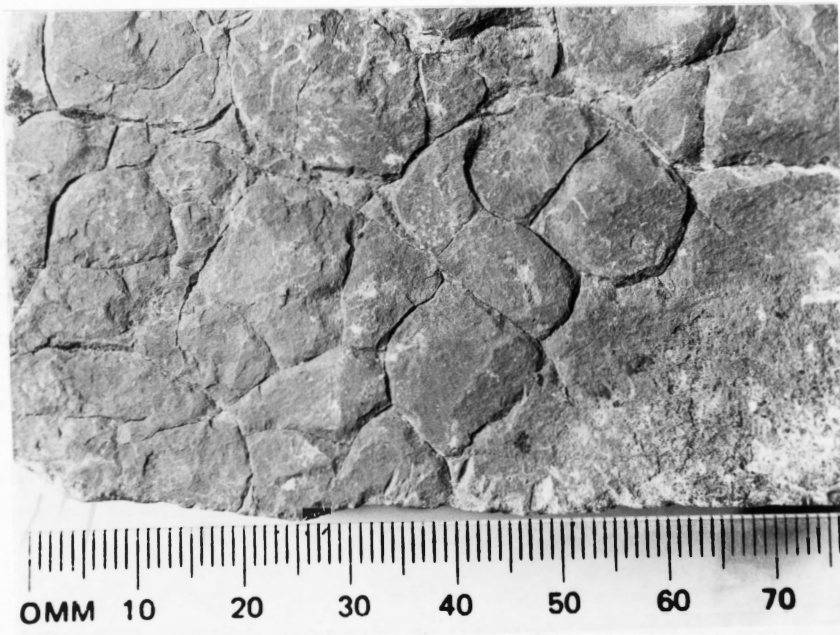


Plate 23. Cracks on the top surface of mudstone strata.

Plate 24. Bioherm of unit 4E, section O (6 m high and 15 m wide).

Plate 25. Plan view of very elongate, columnar stromatolites on the top surface of the unit 4E bioherm shown in Plate 22. (Small divisions on the scale are 10 cm).

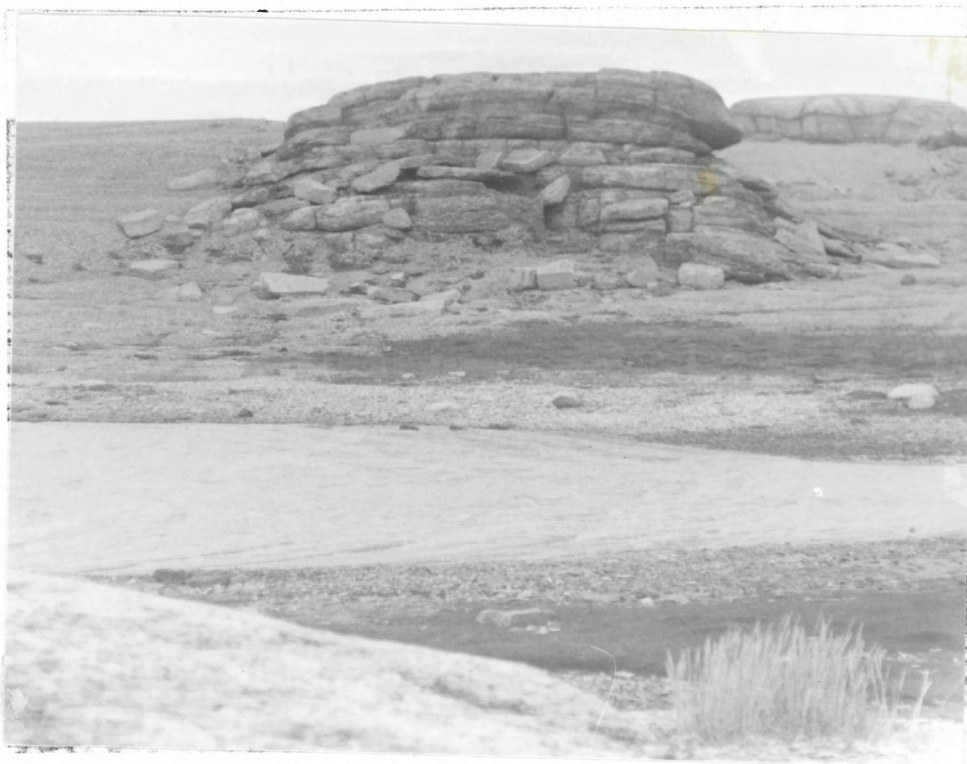


Plate 24

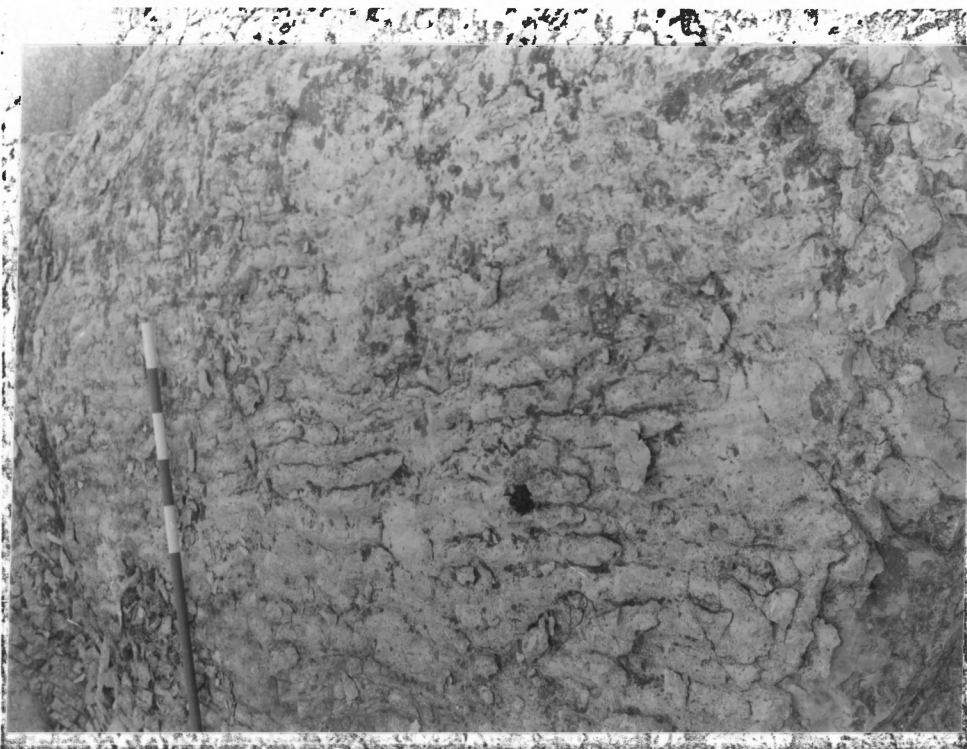


Plate 25

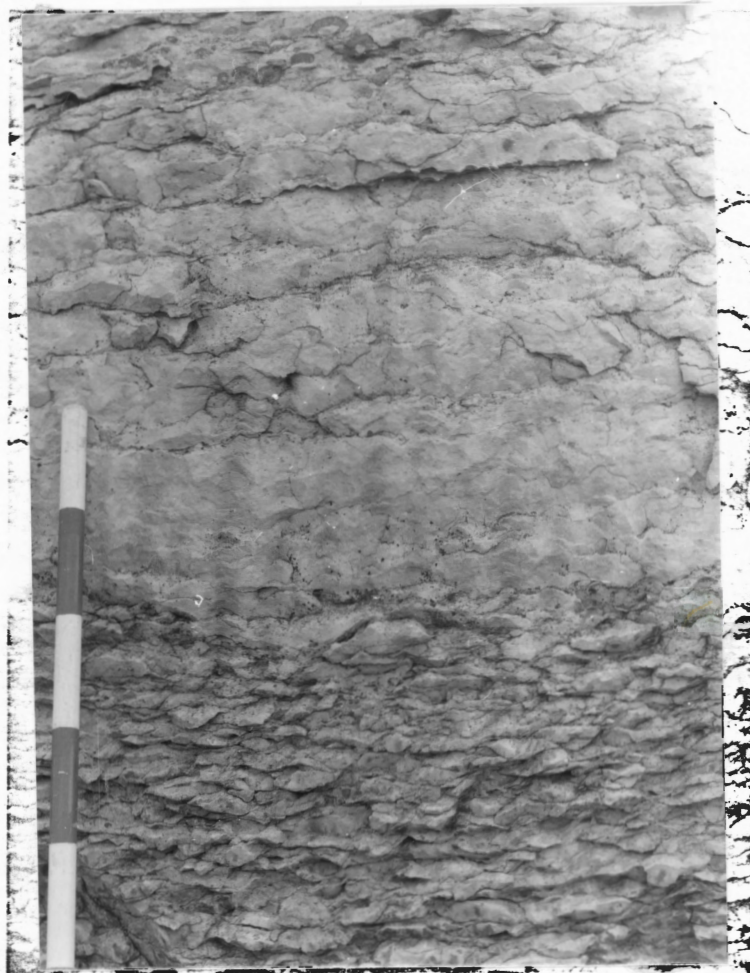


Plate 26. Cross-sectional view of a portion of the upper part of the bioherm. The SH-V with shale partings in the lower portion of the photo grade up into narrow pseudo-columnar-stromatolites. Columns are 3-4 cm in diameter.

columnar stromatolites visible by their darker colour. Near the top of the bioherm, a 20 cm thick bed occurs in which columns are tilted at an angle from the vertical.

Described above is just one of the many large (up to 80 m long and 20 m high) isolated bioherms that lie above unit $4R_4$ (see Table 1). Individual bioherms may be separated by anywhere from approximately 30-50 m rising above the slabby dolomitic drift between.

CHAPTER 3

LABORATORY ANALYSES

A series of laboratory techniques were used on representative samples, from the various units in order to supplement field data, and to gain a better understanding of the composition of the rocks, involved in this study.

Cut Slabs

Thirty-four samples from the various lithologies were slabbed, ground with 100 grit to remove saw marks, and examined. Descriptions of these samples can be found in Appendix 1.

In several instances, structures, not previously visible in the rock, became visible upon slabbing, i.e. stromatolite laminations, cross-laminations, disrupted laminations, and intraclasts. In other cases, slabbing revealed a structureless massive rock (see Appendix 1 for detailed descriptions). Generally, the rocks are red, mauve, or green, with mottles or laminations of the other colours. Small (.1-1 mm), clear, colourless vugs commonly occur in the rocks.

Polished Thin Sections

Twenty-four polished thin sections were surveyed, but 12 of these were examined in more detail, and correspond to samples for which

chemical analyses were done. Descriptions of these 12 thin sections can be found in Appendix 2.

All the rocks have been completely recrystallized and show a crystalline texture. Microstructures are therefore limited, and the major use of the thin sections was for determining relative grain sizes, and the relative amounts of clay, quartz, and hematite.

The dark red rocks, examined in thin section G7 and K2, have a clay matrix with red hematite specks scattered throughout the matrix. These rocks have approximately 2 percent quartz whereas only a few angular, silt-sized, quartz grains were seen in the other thin sections.

Most thin sections have clay and rare opaque specks sparsely disseminated throughout the section. Microstylolites, defined by clay bands extending across the section, are common.

In intraclastic rocks, the grain size of the intraclasts is generally similar to that of the matrix. Lenses of coarser-grained dolomite commonly have inward-increasing grain sizes.

Calcite Staining

Three random thin sections were etched, with .1 m HCl, for various intervals of time up to 5 minutes, and stained with Alizarin Red, a stain for calcite. The stain had no effect on the sections. The technique was tested on a known calcite, which upon staining turned red. The conclusion was that the thin sections stained had no calcite,

and the carbonate was, therefore, assumed to be dolomite.

Insoluble Residue

Four gram portions of 48 sample powders were boiled in approximately 6.5 M HCl for about ten minutes, cooled, and filtered through a dry vacuum flask of known weight. The dry residue was weighted in the vacuum flask, and the weight percent insoluble residue was calculated by comparing its weight with the original sample weight. Results, in weight percent, are plotted in Figure 7, and distributions in the measured sections are shown on Figure 8.

The insoluble residue percentages recorded are only reliable to about $\pm 25\%$ due largely to the tremendous weight difference between the vacuum flask and the sample. However, four runs of sample H10 powders were done, independently, to test the precision of the technique, and results ranged from 8.06% to 10.65%.

Overall results range from 2% to 94%. Within the uncertainty limits discussed above, there are at least three groups: a 7-8% average, a 36% average, and sample K1 alone with 94%.

The composition of the insoluble residue, when examined on a smear slide under a microscope, appeared to be a combination of clay minerals and quartz. No heavy minerals were found.

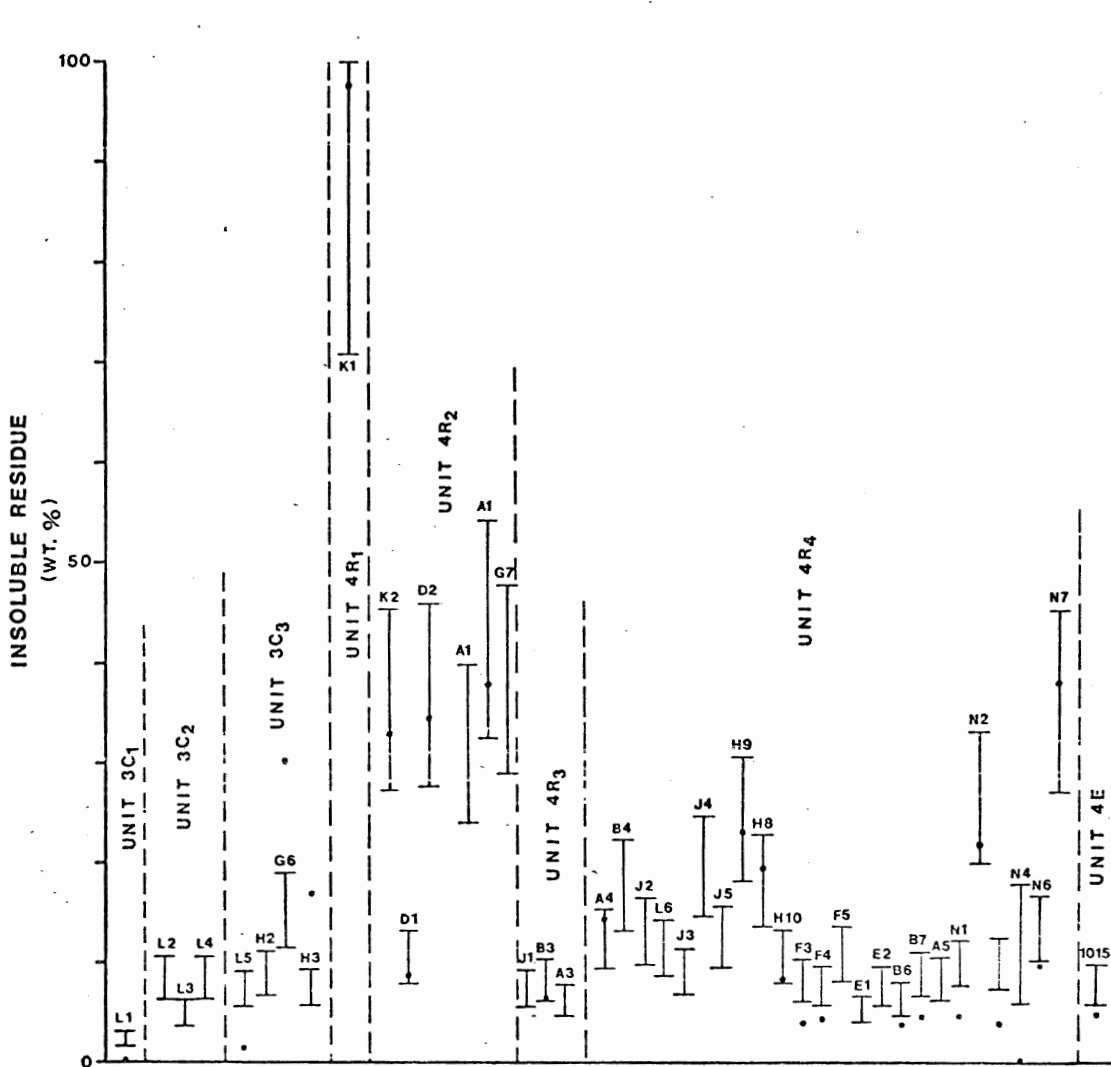
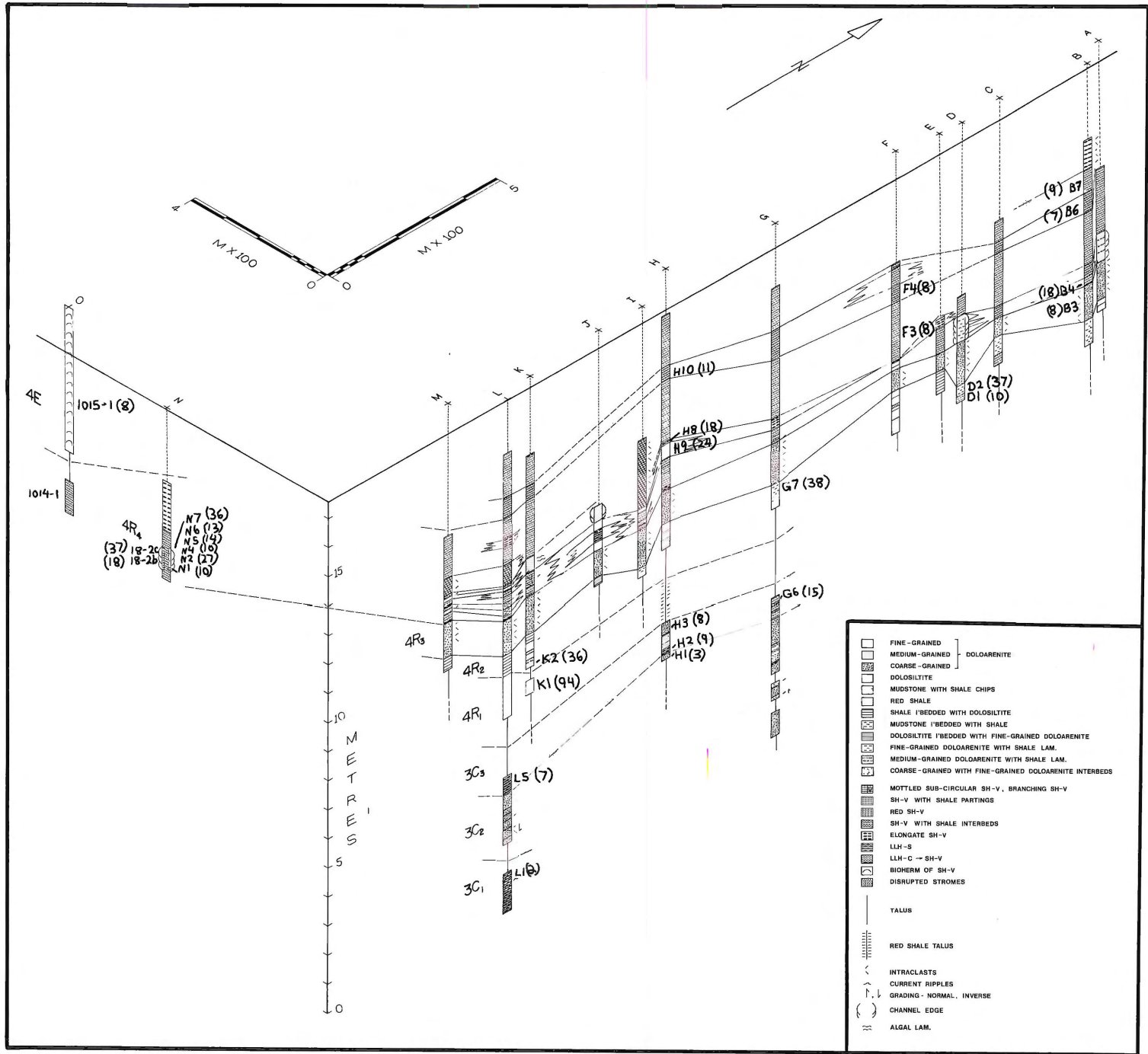


Figure 7. Bar graph of insoluble residues, indicating the uncertainty range, for each sample. The dots represent the calculated insoluble residue percentages.

Figure 8. Fence diagram, showing the stratigraphic position of analyzed samples, and their insoluble residue percentages.

FIGURE 8.



Wet Chemical Analyses

Atomic Absorption analyses were undertaken to analyze for Ca, Mg, Al, Fe, and Mn. 30 sample powders were weighed and digested in HNO_3 , HF and HClO_4 using the standard procedure described in Appendix 3. The samples were heated overnight in a water bath, all but HClO_4 evaporated, fumed in a sand bath until a liquid viscous residue was left, HClO_4 and H_2O added, boiled and cooled, and the resulting liquid diluted to 250 ml. Additional dilutions were necessary to bring the concentrations of the elements in the samples into the ranges for which the Atomic Absorption apparatus could analyze accurately (see Appendix 3). Standard solutions for Ca, Mg, Al, Fe and Mn, as well as sample and standard blanks, were prepared and run for atomic absorption. Weight percentages of each element for the 30 samples were calculated (see Appendix 3a) and tabulated in Table 3. Sample locations are shown on Figure 8.

Analysis for CO_2 was done by acid-base titration, using the procedure described by Grimaldi et al. (1966). 0.2 N HCl was added to 0.5 g of sample and boiled until complete evolution of CO_2 . This was then back titrated with 0.2 N NaOH to find the amount of HCl used in the reaction which then leads to the amount of CO_2 evolved. The detailed procedure is described in Appendix 3b. The weight percent, of CO_2 in each of the 30 samples, is tabulated in Table 3.

The Ca/Mg molar ratio was calculated (see Appendix 3a), and also tabulated in Table 3. The Ca molar percent has been plotted against

TABLE III

Chemical Analyses

(wt%) unless stated otherwise

UNIT	SAMPLE	CaO	MnO	Fe ₂ O ₃ ⁺	MnO	Al ₂ O ₃	CO ₂	CO ₂ calculated	Mole % Ca/Mg	Total Analyses
3C1	L1	28.87	20.95	0.29	.09	.38	45.65	44.38	.99	94.96
3C2	H1	28.50	21.25	0.39	.09	.47	41.51	45.57	.97	96.27
3C3	G6	25.17	9.45	0.57	.10	2.19	39.26	30.07	1.92	67.55
	H2	27.66	15.66	0.62	.08	1.43	42.74	38.80	1.27	84.25
	H3	27.53	13.82	0.80	.11	0.94	42.98	36.69	1.43	79.59
	L5	28.16	20.59	0.37	.11	1.36	42.93	44.58	.98	95.17
4R1	K1	0.31	1.06	1.21	.01	12.79	1.19	1.40	.23	16.48
4R2	D1	26.98	18.21	0.61	.15	1.52	42.19	41.05	1.07	88.52
	D2	18.30	13.97	1.91	.11	6.00	29.11	29.61	.94	69.90
	G7	17.39	13.28	2.58	.09	6.21	27.50	28.15	.94	67.70
	K2	19.16	14.00	0.97	.10	5.53	29.39	30.32	.99	70.08
4R3	B3	26.69	19.62	0.67	.14	1.34	45.75	42.37	.98	90.83
4R4	B4	24.67	17.64	1.01	.14	3.96	38.56	38.62	1.00	86.04
	B7	27.13	19.95	0.81	.14	1.55	42.67	43.07	.98	92.65
	F3	27.81	19.70	0.57	.13	1.45	35.42	43.33	1.01	92.99
	10141	28.81	20.37	0.27	.08	.46	45.70	44.85	1.02	94.83
	F4	27.95	19.41	-	.12	1.45	42.77	43.12	1.04	-
	H10	26.37	18.99	0.53	.11	1.72	43.13	41.43	1.00	89.15
	B6	28.03	19.65	0.75	.14	1.23	41.31	43.45	1.03	93.25
	H8	24.53	15.33	0.91	.12	3.40	37.51	35.99	1.15	80.28
	18-2b	24.54	17.71	0.99	.11	3.30	37.52	38.59	.99	85.24
	18-2c	17.68	13.66	3.04	.09	5.73	27.99	28.79	.93	67.28
	N1	27.60	19.62	0.45	.10	1.73	41.07	43.08	1.01	92.58
	N2	21.27	16.08	1.56	.09	4.83	33.99	34.25	.95	78.08
	N4	32.10	19.51	0.45	.10	1.62	42.37	46.49	1.18	100.3
	N5	25.59	23.97	0.20	.11	2.17	39.78	46.25	1.02	98.29
	N6	25.84	18.83	0.65	.11	2.31	-	40.95	.99	88.69
	N7	18.19	12.41	3.01	.08	5.54	28.77	27.82	1.05	67.05
	H9	21.77	16.17	1.51	.11	4.78	39.95	34.74	.97	79.08
4E	1015-1	27.39	19.17	0.46	.11	1.44	42.38	43.01	1.00	92.15

the Mg mole percent in Figure 9.

As a check for the analyzed CO_2 , the weight percent CO_2 was calculated, and tabulated in Table 3, as that amount used by CaO and MgO to make CaCO_3 and MgCO_3 . An estimated percentage of insoluble residue, assuming that only the CaCO_3 and MgCO_3 were soluble, is plotted with the experimental, insoluble residue in Figure 7.

X-ray Diffraction

Both an unprocessed, sample K1 powder, and the insoluble residue of sample K1 were smeared on glass slides and run for x-ray diffraction. Resultant graphs are shown in Appendix 4. Tentative identification of the minerals, using the peak intensities and the process of elimination of minerals with similarly located peaks, has been attempted. See Appendix 4 for the reasoning behind the following identifications. Relative abundances (Table 4) were estimated by taking the area under the maximum peak, and multiplying by the intensity factor.

TABLE 4

Relative Abundances of Minerals in Sample K1 (by X-ray Diffraction)

Dolomite	.9%;	.7% in insoluble residue
Quartz	9 %	
Plagioclase	5 %	
Muscovite?	12 %	
Orthoclase?	14.3%	
Chlorite?	3 %	

If muscovite is present, then orthoclase and chlorite probably are not present. They occupy the smaller peaks on the x-ray diffraction graph (see Appendix 4). It was hoped that the clay minerals might be identified, but from the results, it is obvious that specialized treatment of the sample would be necessary to allow the clay peaks to be detectable.

DISCUSSION OF LABORATORY RESULTS

Insoluble Residue

The approximate insoluble residue, calculated assuming that all sediment not forming CaCO_3 or MgCO_3 is insoluble, is generally 2 to 4% less than the experimental results for insoluble residue. However, if the degree of uncertainty, (25%), in the experimental results is considered, the calculated value is a very good estimation, in most cases. Sample G6 and perhaps H3, appear to be exceptions. Sample G6, especially, has an experimental, insoluble percentage much lower than the calculated value.

There are several possible reasons for discrepancies in values. The experimental value may be too high, due to incomplete dissolution of the dolomite. The x-ray diffraction results, comparing the mineralogy of a sample before and after boiling in HCl, show the presence of dolomite in both cases, with an only slightly reduced

abundance after boiling! Although such errors are exaggerated in the sample x-rayed, due to the extreme low abundance of original dolomite in that particular sample, it indicates a high probability of a low percentage of dolomite remaining in the insoluble residue. This may partially explain why experimental values are generally slightly higher than the calculated. Low experimental values may be due to dissolution of compounds other than just CaCO_3 and MgCO_3 . The boiling may have caused some clays to dissolve. The yellow colour of the filtrate solution indicates the presence of iron in solution, thus the Fe_2O_3^+ should be calculated as part of the soluble material. However, in the samples with sufficient iron to make any difference to the calculation, this adjustment would then reduce the calculated, insoluble residue to a value too low. Looking at the hand sample or slab for G6 (see Appendix 1), the calculated insoluble residue of 30% seems unreasonable when the sample is compared to other samples with 30% insoluble residue. These other samples are red mudstones, whereas G6 is from a portion of a sub-circular, columnar stromatolite.

Generally, the insoluble residue percentages could be predicted by examining hand samples and thin sections. The light coloured samples are low in insoluble residue, whereas the dark red or brown samples are generally high in insoluble residue. However, colour is not entirely reliable, as indicated by sample H3. Sample H3 is a dark red coarse-grained doloarenite (see Appendix 1), with an experimental insoluble residue of only 8%. The calculated insoluble residue,

17%, might seem more reasonable in this case. However, the rock is coarse-grained, which suggests a lack of fine insoluble residue.

Thin sections of rocks, with high insoluble residue percentages, have quartz grains (2%) scattered throughout the sections. Rocks, with low percentages of insoluble residue, have only occasional quartz grains (trace) in their thin sections.

Ca/Mg Ratio

Ca/Mg molar ratios for the analyzed samples, listed in Table 3, are approximately those of stoichiometric dolomites, 1.00. Figure 9 shows a plot of Ca mole percent versus Mg mole percent. The 1:1 ratio line runs approximately through the bulk of the samples. Samples G6, H3, H2, N4, and H8 are anomalous in having high Ca molar percentages.

Referring back to insoluble residue data, these samples, with the exception of Nr, all had experimental insoluble residues of lower percentages than those calculated. Sample G6 has the highest Ca/Mg ratio, as well as the greatest difference in insoluble residue percentages. Error is not due to the extra Ca forming an insoluble compound, so that the $\text{MgCO}_3 + \text{CaCO}_3$ calculated was too high, because if the amount of $\text{MgCO}_3 + \text{CaCO}_3$ is lowered, the calculated insoluble residue becomes higher.

Sample K1 has an extremely low Ca/Mg ratio, .23, indicating an excess of Mg to that used for dolomite. X-ray diffraction analysis of

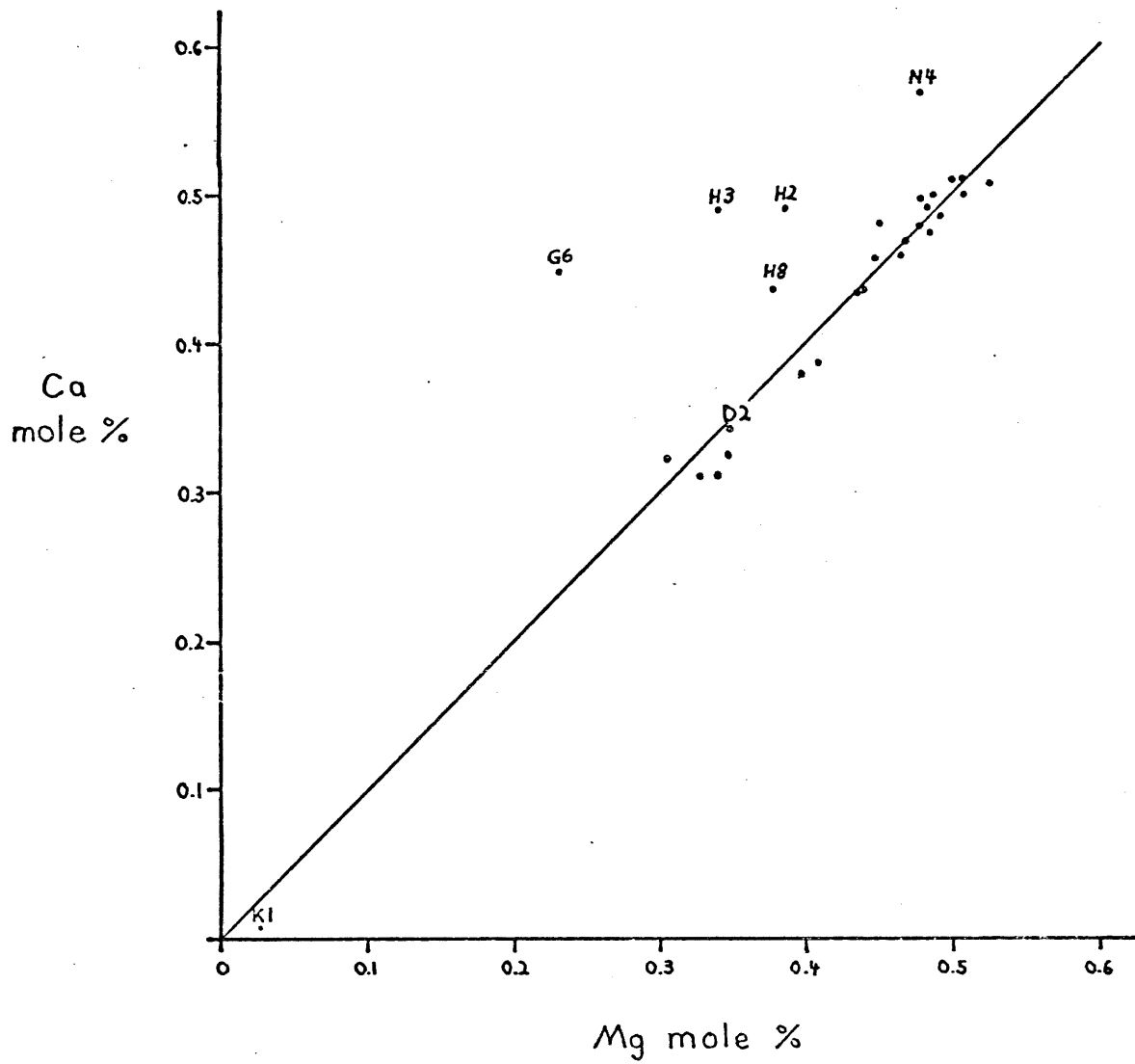


Figure 9. Plot of Ca mole percent versus Mg mole percent, for the thirty analyzed samples. The diagonal line represents the ratio for stoichiometric dolomite.

this sample indicates the Mg might be in either chlorite or muscovite.

Total Iron

Total Fe for the samples, calculated as Fe_2O_3 , is recorded in Table 3. Total Fe is plotted against Al_2O_3 in Figure 10. The samples generally form a linear trend of Fe^{T} increasing with Al_2O_3 . There are seven zones into which the samples fall (see Figure 10). Samples L1, H1, and 1014-1 have low Fe^{T} and low Al_2O_3 . The majority of the samples, fall into a zone with an intermediate range of Fe^{T} and Al_2O_3 . Samples N7, 18-2c, G7 and D2 have high Fe^{T} and high Al_2O_3 . Sample K1 sits by itself with very high Al_2O_3 but not as high Fe^{T} . Sample N5 has an intermediate Al_2O_3 content, but a very low Fe^{T} content.

The amount of Fe^{T} generally corresponds with increasing amounts of Al_2O_3 . The $\text{Fe}/\text{Al}_2\text{O}_3$ ratio, for the clay minerals, is shown in Figure 10 to be lower than that for most of these samples. Thus the Fe, in most samples, occurs as Fe oxide coatings on the clays (Veizer, 1977). Samples K1, K2, and N5 have lower Fe^{T} content, and fall below the $\text{Fe}/\text{Al}_2\text{O}_3$ ratio for the clay minerals illite and montmorillonite. In these samples, it is possible that the Fe^{T} is incorporated in the structure of the clays. However, in studying the thin section for samples N5 and K2, opaque material, probably hematite, was found between grains (see Appendix 2). The dark red colour of sample K1 also suggests iron oxide coatings.

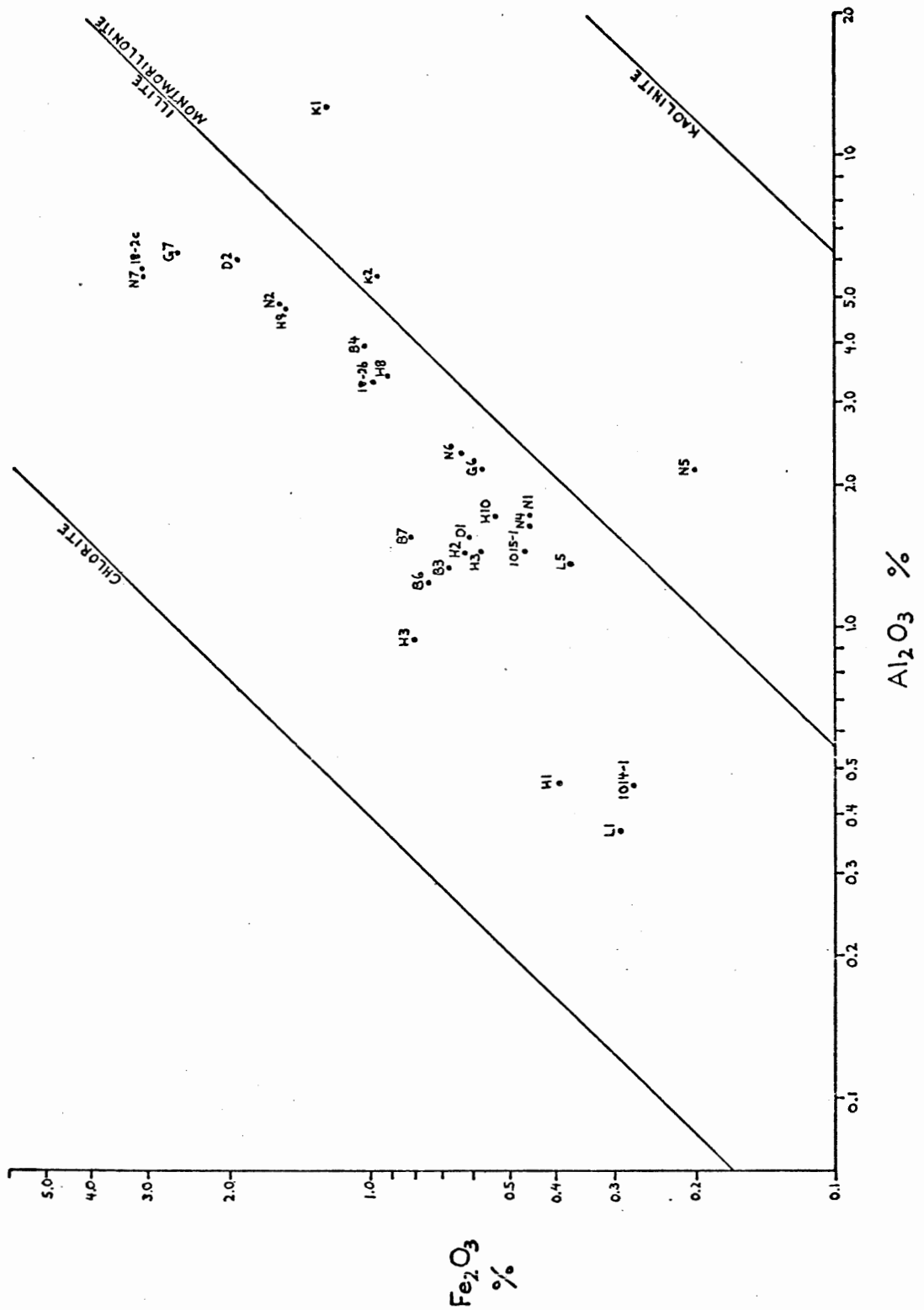


Figure 10. Plot of Fe₂O₃ weight percent versus Al₂O₃ weight percent, for the thirty analyzed samples. The three diagonal parallel lines represent the Fe₂O₃/Al₂O₃ ratios for kaolinite, montmorillonite and illite, and chlorite (from Deer et al., 1964).

Although Fe^{T} has been tabulated completely in the Fe^{3+} , it is obvious, upon examination of the rocks, that some iron is in the Fe^{2+} state. Many of the rocks are red with green mottles or vice versa (see Appendix 1). Many of the mottles are randomly spaced and probably represent local oxidations or reductions of the iron.

Total Analysis Percentage

The sum of the percentages for each analyzed component is presented in Table 3. Although normal chemical analyses added up to 100%, only certain components were analyzed here and hence do not necessarily sum to 100%. SiO_2 , Na, K and H_2O are some major components neglected in the analysis. In many cases, by subtracting the Al_2O_3 percent from the experimental insoluble residue value, and adding this to the total analyses percentage, the result is approximately 100%. This suggests that components, neglected in analyses, occur in the insoluble residue. Of course, one of these is SiO_2 which occurs as quartz, as well as being incorporated in the structure of the clays. Potassium and the hydroxyl radical are probably also important in the insoluble residue, in clays and other hydrous minerals.

CHAPTER 4

ENVIRONMENTAL INTERPRETATION

Units 3C₁ and 3C₂

The coarse-grained dolarenites of Units 3C₁ and 3C₂ may have been deposited in either a constant, medium-energy environment, or in a generally low-energy environment, which received periodic influxes of sediment. The medium-energy environment may be lower intertidal or shallow subtidal, and the low energy environment may be low supratidal, high intertidal, or subtidal (below wave base). A discussion of the validity of each of these, as environments of deposition for Units 3C₁ and 3C₂, is presented below.

Low-Energy Environments

Low Supratidal or High Intertidal

Current indicators, such as ripples and graded bedding, are few, and could be associated with periodic, storm deposition of sediment. Intraclasts, on low supratidal or high intertidal flats, might form on the rock surface by cracking due to prolonged aerial exposure, thus creating a breccia layer. Alternatively, intraclasts could be swept shorewards during storms. The latter explains the size-graded

nature of the intraclastic beds, and the rounding of most intraclasts.

The lack of fine sediment argues against a low-energy supratidal or high intertidal environment, although if deposition was slow, fine mud could have been winnowed out by wind action, or by repeated flood and ebbs. However, the regular, laminar texture of low-domal stromatolites suggests a lower to middle intertidal, rather than an upper intertidal or low supratidal environment (Logan et al., 1974).

Subtidal (below wave base)

Again, the rare ripples and graded bedding represent occasional mechanical deposition, during subsiding storm conditions. Tidal runoff might transport the intraclasts from higher parts of the tidal flats. Lack of fine sediment interbeds, and elongations of stromatolites, might be explained by bottom currents. Oscillation currents indicate that these bottom currents are not unidirectional, and therefore probably not downslope. The coarse-grained dolarenite, then would be deep basinal. However, the intraclasts suggest a position close to a shallow water, turbulent zone.

Medium-Energy Environments

Lower Intertidal or Shallow Subtidal

Preservation of ripples is rare, possibly due to the continuous reworking of the sediment. As mentioned above, intraclasts can be

deposited in lower intertidal to subtidal environments, during subsiding storm conditions. The lack of fine-grained interbeds, in the coarse-grained doloarenite, suggests an energy at least high enough to prevent the settling of fine sediment. The occasional lenses of carbonate mud may represent small, protected depressions in the substrate. Low-domal stromatolites are widely-spaced, elongate, and are composed of regularly laminated coarse-grained doloarenite with fine laminar fenestrae. These are similar to smooth algal mat, stratiform sheets, which Logan et al. (1974) describe growing on lower intertidal to mid-intertidal platforms at Shark Bay. The structureless, coarse-grained doloarenites of Unit 3C₂ may be shallow subtidal deposits, in which stromatolites are rare because mechanical abrasion was too high to permit much permanent binding. The author favours low intertidal to shallow subtidal environments, for Units 3C₁ and 3C₂, because they most easily explain the data available.

Unit 3C₃

The low-domal stromatolites at the base of Unit 3C₃ are similar to those of Unit 3C₁, and as discussed earlier, most likely develop in a lower intertidal environment. Lateral to the low-domal stromatolites are sub-circular, columnar stromatolites, and overlying them are interbeds of dolosiltite in fine-grained doloarenite. The regularly laminated, columnar stromatolites compare to the smooth

mat, columnar structures, described by Logan et al. (1974), occurring in zones with frequent wave turbulence and tidal currents. As the height of smooth algal mat, columnar structures is determined by location with respect to the limiting tide level (Logan et al., 1974), the columnar stromatolites may have grown in the intertidal zone, approximately 20 cm below high tide. The columnar stromatolites are probably higher than the low-domal stromatolites, in a zone where turbulence is greater. The dolosiltite represents a protected environment, possibly a depression or a zone protected by a hydraulic barrier. Perhaps the columnar stromatolites cause this hydraulic barrier effect. The validity of this statement depends on whether the dolosiltite and the columnar stromatolites are more than just local pods, and whether one grades laterally into the other.

Some of the geochemistry of the upper part of Unit 3C₃ is anomalous, in that two samples, G6 and H3, have experimental insoluble residues lower than that calculated from chemical data (see Chapter 3). All samples from the section, were treated the same, and only these two samples show such a great difference. The difference in insoluble residues may have been caused by solution of clays. Since only samples G6 and H3 were affected, this suggests that these two samples contain a clay mineral that is more soluble in boiling acid, than clays in other samples from the section. If this hypothesis is correct, then a clay source, different from other units, is suggested

for the upper portion of Unit $3C_3$. Alternatively, local chemical anomalies, in the water, may have transformed the deposited clay, or other insoluble sediment, into a more soluble form.

Local chemical differences are suggested by the Ca/Mg ratios for the columnar stromatolites (Sample G6), and the red, coarse-grained dolomarenite (Sample H3) (see Figure 9). Both ratios are anomalously high (G6 = 1.92 and H3 = 1.43). The higher Ca/Mg ratio may reflect a temporary decrease in salinity, due to an influx of fresh water or less restricted circulation at the depository. However, if the dolomite is a later diagenetic phenomenon, then the higher ratios may simply represent local differences in the diagenetic fluid. The recrystallized nature of the rocks, in the study section, suggests a diagenetic or metamorphic origin for the dolomite, but the process of dolomitization of large ancient carbonate deposits is not fully understood at present.

In summary, Unit $3C_3$ probably represents a lower intertidal flat with irregular topography. Columnar stromatolites, dolosiltites, and geochemical anomalies might be explained by topographic highs and lows.

Units $4R_1$, $4R_2$, and $4R_3$

Shale, Dolosiltite and Intraclasts

Parallel-laminated mudstone, shale, and dolosiltite occur in a quiet environment, such that fine material can settle out of

suspension. There are several ways in which an environment might be protected from wave agitation. Supratidal mud flats are protected by their position above mean high tide level. Lagoons are quiet environments due to subaerial bars. Low energy environments can also be formed by the hydrologic effect of a shelf edge, or a certain point on a gently sloping bottom, where the shallowing floor causes waves to break and dissipate most of their energy, before entering shallower water. Finally, mud can accumulate in relatively deep water below wave base, either in tidal ponds or offshore (Heckel, 1972).

Determination of the environment of formation for shale is difficult in Precambrian rocks, where biota is absent. The presence of possible mudcracks in the shale suggests intermittent subaerial exposure. Hematite coatings on the sediments indicate oxygenated conditions, most often subaerial, but deep sea sediments may also be oxygenated (Dunbar and Rodgers, 1957).

The shale strata are composed of approximately 5 percent carbonate (sample K1, Figure 7 and 8), suggesting either slow deposition, or a rapid deposition of clays. The fine-grained doloarenites, and dolosiltites, overlying the shale, have approximately 65 percent soluble carbonate (see Figure 8). The interbeds of shale, with the dolo-siltite, indicate fluctuation of conditions, either rapid influxes of terrigenous mud, or constant settling of terrigenous mud and periodic breaks in carbonate deposition. Determination of the most probable

of these two mechanisms depends on the environment in which the shale is located.

Deep Water

The subtidal (below wave base) environment is one in which shale might be deposited. The clay could travel in suspension, across the turbulent tidal flat, and be deposited where the gradually sloping platform reaches depths below wave base. In this case, cracks on the shale surface must have formed by some unknown process, not dessication. This is possible as the cracks have a form unusual for subaerial mudcracks.

Strata of Units $4R_1$ and $4R_2$ are similar in lithology to planar, thin beds of carbonate siltstone or mudstone in the Kuvik Formation at Bathurst Inlet (Cecile and Campbell, 1978). These grade upward into green-gray and red, argillaceous mudstones, interstratified with thin beds of uniform mudstones, carbonate, or laminated carbonates. This sequence was interpreted as being deposited in deep water near the base of a carbonate shelf margin, or a shallow carbonate platform (Cecile and Campbell, 1978). Sedimentary structures include climbing ripples, slumps, scours, graded bedding, and cross-laminations in calc-siltite. Most of these structures were not seen in the study section. As it is largely from the sedimentary structures that Cecile and Campbell (1978) determined the deep-water origin of the mudstones, it is not possible to conclude that the mudstones in the study section were definitely deposited in deep-water.

One possible supporting factor, for a deep-water origin of the Unit 4R mudstones, is the sudden appearance of red mud in Unit 4R, the first since the base of the Parry Bay Formation. The conical stromatolites, of the P_{3B} member (Table 1), mark a change from the shallowing and deepening-upward cycles, discontinuous units of stromatolites, oolite shoals, and intraclast-bearing dolarenite of the lower Parry Bay Formation, to strata characterized by vast, thick, uniformly elongate stromatolite sequences (Campbell, 1979). Campbell (1979) has interpreted the rocks below the conical stromatolites as being deposited on an intertidal platform. The conical stromatolites suggest the beginning of a marked change in environmental conditions. Thus, if Campbell's interpretation of the lower Parry Bay Formation is correct, then the study section may represent a subtidal environment. However, in this case, a higher intertidal to supratidal environment is equally possible.

Low Supratidal

Possible mudcracks suggest a low supratidal origin for the shale-dolosiltite strata. The dolomitic sediment was probably deposited during periods of very high tides and the shale could be supplied by an ephemeral stream. In this case, alternating periods of rapid sedimentation of terrigenous clay and marine carbonate occurred.

Alternatively, the terrigenous clay may have been supplied constantly by a slow stream, while the carbonate was only deposited

during periods of very high tides.

Salt and gypsum casts were not found in these rocks, but conditions may not have been right for their precipitation or preservation. However, it is unlikely that recrystallization of the dolomites would destroy salt or gypsum structures, as such structures have commonly been found in similar rocks at the base of the Parry Bay Formation.

The intraclastic strata, overlying the fine-grained sediments, may have been washed shorewards and deposited on supratidal flats during storms, and the shale deposited again as storm energy diminished.

Intertidal

A shallow lagoonal origin for the shales and dolosiltite is possible, but evidence for a sub-aerial barrier is not present in the study section. However, a hydraulic barrier, on a gently sloping bottom, producing a similar effect, is highly possible. Normal deposition might be the settling of fine-grained material, while storms may cause intraclasts to be washed over the hydraulic barrier.

With the available data, a low supratidal environment, or an area protected by a hydraulic barrier, on a gently sloping bottom, are equally valid. The supratidal model best explains the abundance of clay, while the hydraulic barrier model best explains the absence of evaporites.

UNIT 4R₄

There are two major environments in which stromatolites might develop, deep-water or shallow-water. Because knowledge of ancient stromatolitic environments is limited, especially those of Precambrian age, either one is possible. The fact that grazing organisms were not present in the Precambrian, greatly expands the environments in which algal mats might have survived. A discussion of the validity of each environment, for the stromatolites of the study section, is presented below.

Deep-Water Sedimentation

There are a few instances in which ancient stromatolites have been interpreted as deep-water, due to the deep-water nature of surrounding sediments. Hoffman (1974) describes circular columnar stromatolites of Lower Proterozoic age at Great Slave Lake. Columns are linked with reliefs of only 2 to 3 cm above the surrounding mudstone. These have been interpreted as deep-water stromatolites (at least 10's of feet deep), because they are interstratified with, and extend beyond the downslope end of the graywacke-turbidite and basin slope facies. The cross-sections of elongate stromatolites in the study section are similar to the cross-sections of Hoffman's deep-water stromatolites. However, siliclastic mud does not occur between the columns, and the stromatolites of the study section are elongated, rather than circular.

Playford et al. (1976) suggest criteria for deep-water stromatolites, from their study of stromatolites in the Devonian-aged, Canning Basin of Australia. These criteria include the absence of fenestral fabric, and the presence of fine laminations, condensed sequences, depositional slopes, drowned reefs, allochthonous blocks, pelagic faunas, iron and manganese precipitation and a red colour (Playford et al., 1976). Although the stromatolites in the study section have many of these characteristics, similar criteria can be used to argue either a deep-water or a shallow-water origin. For example, Logan et al. (1974) found lower intertidal stromatolites with fine laminations, in condensed sequences. Apparent sub-vertical growth of stromatolites may either represent the actual growth angle of the stromatolites, or may indicate vertical growth on a depositional slope. A red colour, due to oxidation, is more commonly due to sub-aerial exposure, than to deep-water oxygenated conditions. Thus, since evidence for drowned reefs, allochthonous blocks, pelagic faunas, and significant iron and manganese precipitation, is absent in the study section, stromatolites in Unit 4R₄ may be either deep-water or shallow water in origin.

Recent, subtidal columns and ridges, near Carbla Point in Hamelin Pool, extend to depths of about 2 metres. However, because of their present corroded nature, it is disputed whether these stromatolites actually grew in a subtidal environment. Local tectonic submergence, of intertidal stromatolites, might put relict intertidal structures into a subtidal environment (Logan et al., 1974).

It is possible that conical stromatolites, of the P_{3B} member of the Parry Bay Formation, underlying the study section (see Table 1), are subtidal. Donaldson (1976) has interpreted conical stromatolites, of the Helikian-aged Dismal Lakes Group in the Northwest Territories, as subtidal, because of the undecapitated cones, the lack of inter-column detritus, the purity of the carbonate, and the lack of sedimentary structures indicative of waves, strong currents or sub-aerial exposure. Conical stromatolites, of the P_{3B} member, are similar in size and purity to those described by Donaldson. However, intraclastic detritus commonly occurs between cones, and gradations between domal and conical laminations are common (Campbell, 1979, and personal observation). Thus, these conical stromatolites show characteristics compatible with turbulent conditions, and a shallow subtidal or intertidal environment may be inferred.

It is possible that stromatolites in the study section are subtidal, but there is no exclusive evidence for such a conclusion.

Shallow-Water Stromatolites

The algal structures in the study section have fairly regular convex laminations, about 1 mm thick. Regular laminations are characteristic of smooth algal mats which occur in Hamelin Pool, in a zone ranging from 1 m below prevailing low-water level to middle intertidal (Logan *et al.*, 1974). Smooth algal mats can develop into stratiform sheets, ridge and rill structures, or discrete columnar

structures. These are all represented in the study section.

Much of the base of Unit 4R₄ consists of low-domal undulations, with adjacent domes linked by continuous laminations (LLH arrangement) (see Figure 6 and Plate 8). Laminations are about .5 to 1 cm thick and synoptic relief is about 2 cm. These stratiform sheets are found in areas of prevailing low energy on gentle, smooth slopes at Shark Bay (Logan et al., 1974). The smooth mat, stratiform sheets at Shark Bay occur in the lower intertidal zone, and their relief is generally lower than the tidal range. Stratiform sheets in low energy, higher intertidal areas could be expected to have a pustular texture, rather than the regular laminations of the LLH in the study section.

Intraclasts, interrupting the normal stratiform layering, might represent periods of prolonged sub-aerial exposure of the mats, causing dessication and brecciation. This suggests a higher intertidal location for the stratiform sheets. Intraclasts, on lower intertidal, stratiform sheets, would represent subsiding storm conditions, when tidal runoff transported intraclasts from higher parts of the flat (Logan et al., 1974). This latter is favoured, as intraclasts are generally rounded.

The stratiform sheets are most often gradational into the elongate stromatolites (Figure 6), which are comparable to the smooth mat, ridge and rill structures described by Logan et al. (1974). The structure is initiated by wave scour and maintained by localization of

wave currents and tidal runoff in the rills. Constant, northwest-southeast, elongation directions indicate northwest-southeast currents, and a northeast-southwest trending shoreline. Ridge-rill structures, in Hamelin Pool, are mainly at the seaward margins of prograding sheets, where the locally steepened depositional slope promotes tidal runoff and/or waves, but they can also occur in interiors of tidal flats, where large columns of tidal water produce significant scour (Logan et al., 1974).

Ridge-rill structures in the lower portion of Unit $4R_4$ are relatively low in height, and are surrounded by sub-circular stromatolites. These, most likely, occur on high parts of the tidal flat. There are two possible origins for the ridge-rill structures in the upper portion of Unit $4R_4$ and Unit 4E. They may represent filling up of an intertidal basin, causing restriction of tidal movement and tidal range. This restriction would cause water to be channelled. On the other hand, Logan et al. (1974) found that the height of ridges increased with the lowering of the intertidal surface. The heights of the ridges in Unit $4R_4$ range from 13 cm in the lower portion of the unit, through 60 cm in the upper portion, to over 2 m in the isolated mound, but the synoptic relief is never more than a few centimetres. Thus, the increasing height suggests a gradual subsidence, beginning near the top of Unit $4R_4$. Large channels could form in both models, either by restriction of large volumes of water in the former, or by a locally steepened slope in the latter. Both models are possible, but due to the upwards increasing heights of the ridges,

the gradual subsidence model is favoured.

Discrete, sub-circular, columnar structures both underlie, and overlie, the ridge and rill structures in Unit 4R₄ (see Figure 6). Smooth mat, columnar structures, at Hamelin Pool, occur in zones with frequent wave turbulence and tidal currents. Their height is determined with respect to the limiting tide level (Logan et al., 1974). The columnar stromatolites in the study section have a moderate relief (less than 20 cm), suggesting that the stromatolites occur fairly high on the intertidal flat, perhaps middle intertidal, and that the depositional slope was shallow. If the slope was steep, then an increase in relief of the stromatolites downslope would be notable.

Sub-aerial exposure is suggested by the common occurrence of intraclasts between both stromatolite columns and ridges. The thin plates oriented sub-vertically between some stromatolites, in Unit 4R₄ (see Plate 17), may have been formed by dessication of the upper portion of the stromatolites, and rinds spalling into the interareas. However, bioerosion by algae or incomplete/discontinuous cementation might produce similar thin plates.

Medium-grained, and fine-grained dolarenite lenses occurring between stromatolitic strata may represent channels. The absence of cross-beds suggests that the channels were formed by currents which carried their sediment load through the channel, and that sediment was deposited only after energy diminished. Alternatively, the medium, and fine-grained dolarenite may have been deposited in depressions, or on topographic highs, on a tidal flat. Their deposition requires

conditions unfavourable for stromatolite growth and the shale laminations suggest periods of quiet conditions. It is also possible that the parallel-bedded, medium-grained dolarenites represent zones of stratiform, smooth algal mats, which grade laterally into columnar structures.

Shale and mudstone lenses in Unit $4R_4$ possibly represent infilled tidal channels, or shallow tidal ponds. If oval cracks on the upper surface of shale strata in Section H (see Figure 3) are mudcracks due to dessication, then an intertidal environment is suggested.

The isolated mound, near the top of Unit $4R_4$, may have been created by channels cutting down into ridge-rill strata, isolating the mound. Shallowing of the water, may have permitted the columnar stromatolites to build up around the mound. Alternatively, the mound may represent a relict tidal channel, cut into tabular sheets of sub-circular stromatolites. After cutting the channel, current energy decreased and low-domal stromatolites grew on the channel floor. As energy decreased still more, stromatolites became smaller, and lower in relief, forming the pseudo-columns. Elongations of the stromatolites might represent the last remnants of a current. This hypothesis is supported by the channel-like shape of the mound and is the preferred, because of the greater extent of the columnar stromatolites, than the ridge-rill stromatolites, in Unit $4R_4$.

UNIT 4E

The lack of total exposure, of the bioherm examined, permits a number of genetic interpretations. The bioherms of Unit 4E may have grown as large broad structures with a relief of several metres, or they may have developed at a similar rate to the channels between, such that the bioherms barely stood above the surrounding sediment. Hoffman (1976) describes an alternate mode of formation, described below.

Large bioherms occur within 1 to 5 km of the outer edge of an Aphebian-aged carbonate shelf, in the Northwestern Canadian Shield. There, stromatolites originally formed in a tabular sheet, in shallowing upward sequences. Apparent stromatolite bioherms were formed by tidal channels, cutting down into the stromatolite sheet, to develop depressions filled with cross-bedded, intraclastic grainstone. The bioherms and their constituent columns were generally elongate normal to the shelf edge, and stood several metres above the channel floor. Tidal channels widened towards the shelf edge, at the expense of the bioherms. The tabular strata of the bioherm described in Unit 4E (Plate 23) may have formed by a similar process. The great heights of the ridge and rill structures, prominent in the bioherm (Plate 24), suggest location at the edge of a subsiding tidal platform of steepening slope.

CHAPTER 5

CONCLUSION

There are a number of feasible interpretations for each unit of the study section, but with the limited data available, and the present knowledge of stromatolites, the following environment is preferred.

The sediments of the study section were deposited on a shallow-sloping, tidal platform with a northeast-southwest trending shore line. The various units were positioned as shown in Figure 11. Because of the shallow slope of the platform, small fluctuations in sea level could cause dramatic transgressions or regressions. At the base of the study section, the coarse-grained dolarenites, of Units $3C_1$ and $3C_2$, were deposited in lower intertidal, and shallow subtidal conditions, respectively. The varied lithologies, of Unit $3C_3$, represent an irregular, lower intertidal surface. Following a regression, shales and mudstones, of Units $4R_1$ and $4R_2$, were deposited in a quiet environment behind a hydraulic barrier, or on a supratidal flat, and were periodically covered by intraclasts (Unit $4R_3$) during storms.

Columnar, and ridge-rill stromatolitic structures of moderate relief occupy a middle intertidal zone. Near the top of Unit $4R_4$, subsidence of ridge-rill structures took place, at the edge of the platform. This caused the incision of platform stromatolites by tidal currents, to form large channels and apparent bioherms.

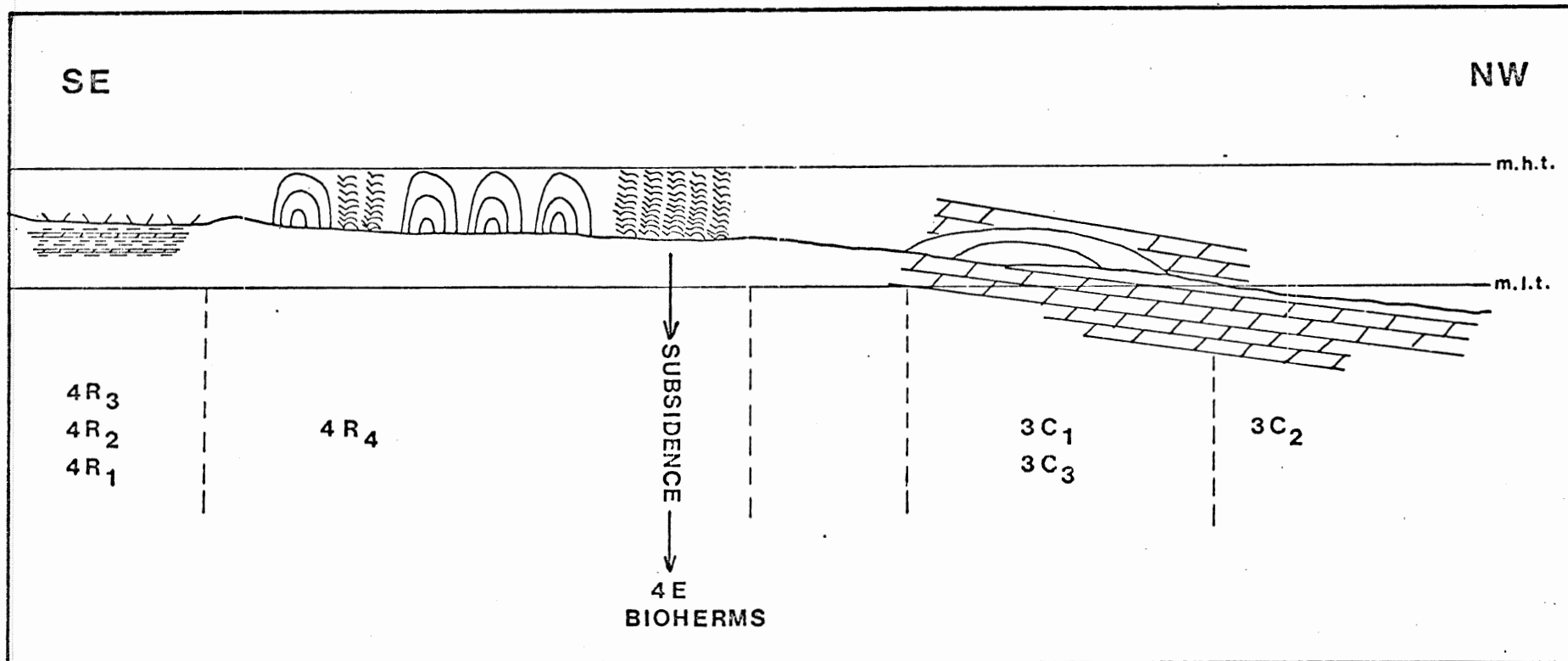


Figure 11. Schematic diagram of the depositional environment interpreted from the study section.

REFERENCES

- Campbell, F.H.A., 1978. Geology of the Helikian Rocks of the Bathurst Inlet Area, Coronation Gulf, Northwest Territories. G.S.C. Paper 78-1A, p. 97-106.
- Campbell, F.H.A., 1979. Stratigraphy and Sedimentation in the Helikian Elu Basin and Hiukitak Platform, Bathurst Inlet-Melville Sound, Northwest Territories. G.S.C. Paper - in press.
- Cecile, M. P. and Campbell, F.H.A., 1978. Regressive Stromatolite Reefs and Associated Facies, Middle Goulburn Group (Lower Proterozoic), in Kilohigok Basin, N.W.T.: An Example of Environmental Control of Stromatolite Forms. Bull. of Canadian Petroleum Geology, vol. 26, no. 2, p. 237-267.
- Deer, W. A., Howie, R. A. and Zussman, J., 1964. Rock forming minerals, vol. 3, 4. Longman, London, 270 pp. and 435 pp.
- Donaldson, J. A., 1976. Paleoecology of Conophyton and Associated stromatolites in the Precambrian Dismal Lakes and Rae Groups, Canada. IN Stromatolites (ed. Walter, M. R.) Developments in Sedimentology 20, Elsevier Scientific Publishing Co., N.Y. pp. 523-534.
- Dunbar, C. O., and Rodgers, J., 1957. Principles of Stratigraphy. John Wiley and Sons, Inc., N.Y., 356 pp.
- Fraser, J. A., 1964. Geological notes on the northeastern District of MacKenzie. G.S.C. Paper 63-40, 1 map, 20 p.
- Grimaldi, F. S., Shapiro, L., and Schnepfe, M., 1966. Determination of Carbon Dioxide in Limestone and Dolomite by Acid-Base Titration. U. S. Geol. Survey Prof. Paper 550-B, p. B186-B188.
- Heckel, P. H., 1972. Recognition of Ancient Shallow Marine Environments. IN Recognition of Ancient Sedimentary Environments (ed. J. K. Rigby and Wm. K. Hamblin). Society of Economic Paleontologists and Mineralogists, Spec. Pub. No. 16, pp. 226-286.
- Hoffman, P., 1974. Shallow and deep water stromatolites in Lower Proterozoic platform-to-basin facies changes, Great Slave Lake, Canada. Amer. Assoc. Petrol. Geol. Bull., v. 58, p. 856-867.
- Hoffman, P., 1976. Environmental Diversity of Middle Precambrian Stromatolites. IN Stromatolites (ed. Walter, M. R.) Developments in Sedimentology 20. Elsevier Scientific Publishing Co., N. Y. pp. 599-611.

- Logan, B.W., Rezak, R., and Ginsburg, R. N., 1964. Classification and Environmental Significance of Algal Stromatolites. *Jour. Geol.*, v. 82, p. 68-83.
- O'Neill, J. J., 1924. The geology of the Arctic coast of Canada, west of Kent Peninsula. IN Report of the Canadian Arctic Expedition, 1913-1918; Southern Party - 1913-1916; vol. XI, Geology and Geography, Part A, 107 p., 1 map.
- Piper, D.J.W., 1977. Manual of Sedimentological Techniques. Dept. of Geology and Oceanography, Dalhousie University, Halifax, N. S.
- Playford, P. E., Cockbain, A. E., Druce, E. C., and Wray, J. L., 1976. Devonian Stromatolites from the Canning Basin, Western Australia. IN Stromatolites (ed. Walter, M. R.) *Developments in Sedimentology* 20. Elsevier Scientific Publishing Co., N.Y. pp. 543-563.
- Veizer, Jan, 1978. Secular Variations in the Composition of Sedimentary Carbonate Rocks II. Fe, Mn, Ca, Mg, Si and Minor Constituents. *Precambrian Research*, 6, pp. 381-413.
- Walter, M. R., 1976. Stromatolites. *Developments in Sedimentology* 20. Elsevier Scientific Publishing Co., N. Y.

APPENDICES

- Appendix 1 Sample Descriptions
- Appendix 2 Thin Section Descriptions
- Appendix 3 Wet Chemical Analysis
- 3a Atomic Absorption
- 3b CO₂ analysis, Acid-Base Titration
- Appendix 4 Determination of Minerals Using X-ray Diffraction

APPENDIX 1

Sample Descriptions

Following are descriptions of representative samples from the various lithosomes.

Unit 3C₁

Sample L1 is a massive, structureless, clear white, coarse-grained doloarenite.

Unit 3C₂

Sample L3 shows a reddish-coloured, intraclastic layer cutting irregularly down into a green lime mud layer. Small, 3mm long, lath shape and 2 mm diameter, rounded intraclasts grade upwards into long, thin, finely laminated intraclasts, 20 by 1 mm, lying at oblique angles to the bedding. Intraclasts are fine-grained and greenish in colour, while the matrix is coarse-grained and reddish in colour.

Sample L4 is basically a greeny grey, with some red, coarse-grained doloarenite. It is parallel laminated with alternating green, light green, and reddish laminations. One dark green lamination, 2 mm thick, has black specks throughout the layer. This layer pinches out within the sample. The laminated portion of the

sample grades upwards into an intraclastic zone, with spaces between intraclasts filled with a clear, colourless dolomite.

This zone is again overlain by parallel laminations.

Sample G4 is a greeny-grey, coarse-grained doloarenite with disrupted laminations, giving it a mottled appearance. Some black specks occur in a darker green lense. A lime mud layer occurs at the bottom of the sample with an irregular contact.

Sample G5 is a reddish-grey, coarse-grained doloarenite with intraclasts. Intraclasts at the bottom of the sample are finely laminated laths, 25 by 2 mm in size, lying parallel to the bedding. These grade upwards into smaller, rounded, lath-shaped or elliptical, randomly oriented intraclasts, 3 x 1 mm in size. Intraclasts are finer-grained than the matrix.

Sample H1 is a grey coloured, coarse-grained doloarenite with clear red, filled cavities. Laminations are wavy and filled-cavities are oriented parallel to the laminations, and follow their general trend.

Unit 3C₃

Sample H2 is dark green with thin, light green, convex-upwards laminations. Laminations are continuous but rather wispy. Red, wispy mottles also occur.

Sample H3 is a dark red coloured, coarse-grained doloarenite. Continuous flat laminations along the bottom of the sample are interlayered with thin (.1-1 mm) lenses of clear colourless

dolomite. Upwards in the sample the laminations are broken and replaced by short, convex laminations sloping downwards. On the top surface of the sample, the bedding plane, are 1 mm wide ridges, approximately 1 mm in relief, 25 mm in length and spaced 16-21 mm apart. When examined closely, two sets of ridges, differently oriented, can be seen superimposed on the main set. One of these sets is 9 mm wide, spaced 12 mm apart, and the other set is 2 mm wide but rare.

Sample L5 is finer-grained than sample H2. Grey-green and red, .1 mm thick, laminations are wavy and convex upwards. On one side of the sample, these laminations are cut off by a steep set of cross laminations.

Sample G6 is the upper domal surface of one of the sub-circular columnar stromatolites. Laminations end abruptly at the edge of the stromatolites, forming a straight vertical wall. Laminations are green with reddish-green and red mottles between laminations. Interstromatolite material is coarser-grained and massive with red and green tiny mottles.

Unit 4R₁

Sample K1 is a thin bedded, laminated, highly friable, red calcareous shale. Some layers of the sample are green.

Unit 4R₂

Sample A1 is a red mudstone with green mottles. Cross laminations are present.

Sample B1 is a red-coloured mudstone with green mottles. Bedding is graded, coarser-grained at the bottom, becomes cross-laminated, and finally is finer-grained near the top of the sample.

Sample F1 has alternating, light green and thin, dark green and red laminations, which are convex horizontally to the south (see Plate 4). The photo shows disrupted laminations to the right, and continuous laminations to the left. These laminations begin being peaked, and gradually become more rounded leftwards. The wall of the laminations is well-defined and a second smaller set of laminations occurs below the larger.

Sample G7 is a dark red fine-grained mudstone with a few green mottles, but otherwise structureless.

Sample H4 is a structureless, green dolosiltite.

Sample K2 is a red, fine-grained doloarenite with green mottles.

The dark red colour at the bottom of the sample changes sharply to a lighter red at the top of the sample.

Unit 4R₃

Samples B3, J1, and I1 are red and green coarse-grained doloarenites with intraclasts. Intraclasts range from 3 x 1 mm to 42 x 3 mm in size. Intraclasts are most commonly green, while the matrix is

reddish.

Unit 4R₄

Sample F3 is a red (mauve) and green mottled, fine-grained doloarenite.

Discontinuous wispy laminations are convex upwards and are irregular alternations of red and green wisps. The rock is basically red with green mottles of a few centimetres diameter. One mm diameter black spots are widely scattered over the cut surface of the rock.

Sample B7 is a mauve-red coloured, convex-laminated, fine-grained doloarenite. Black spots, possible clear, colourless dolomite, up to 3 mm diameter, are common.

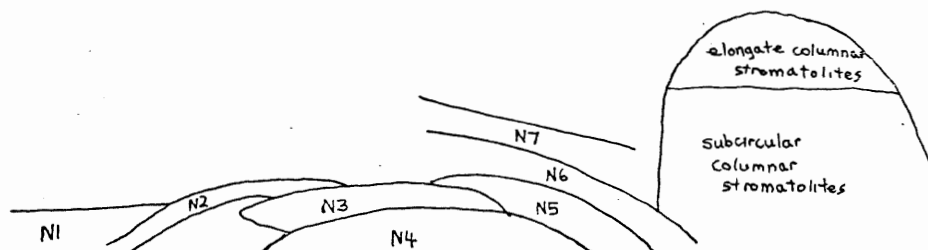
Sample H10 is a mauve coloured, convex-upward laminated, fine-grained doloarenite. Laminations are faintly visible alternations of very thin, light and dark mauve laminations. In places, a green mottling follows the laminations as curved wispy streaks but in other places, it occurs as green patches (5 mm diameter). Both dark red and clear, colourless, filled cavities occur either as discontinuous streaks following the trend of the laminations, or as oblong patches several millimeter in length. The clear colourless patches are dark red around some portion of their edges.

Sample H8 is a mottled mauve and green, fine-grained doloarenite. In the section cut no laminations can be seen. Dark red spots and lenses 3 mm by .5 mm, occur both in the mauve and green portions of the rock. The red and green colourations appear random.

Sample 18-2b is a mottled red and green, fine-grained dolarenite with slight undulous lamination.

Sample 18-2c is a red mudstone. A 7 mm thick layer of alternating light red, 2 mm thick, and dark red, 1 mm thick laminations is distinctive in the sample. The light red laminations are themselves, very finely laminated. Aside from this layer, the mudstone is structureless.

Samples N1 to N7 were taken from a complex of layers diagrammed below. See Plate 21.



Sample N1 is a green fine-grained dolarenite with some discontinuous, poorly developed laminations defined by fine, reddish bands.

A zone of small (2 mm long) clear colourless, filled, elongate cavities occurs above the laminations.

Sample N2 is a massive, structureless, red mudstone.

Sample N4 is a fine-grained dolarenite with intraclasts. The intraclasts are green and the matrix between them is pinkish green. Some streaks of darker green appear as laminations, extending across the sample, slightly convex upwards.

Sample N5 is a red, fine-grained doloarenite with dark red streaks and lenses oriented parallel to the laminations. These dark red patches appear to define a fine fenestral fabric. The sample is mottled green in random locations.

Sample N6 is a green and light red coloured, very faintly, finely laminated, fine-grained doloarenite. It is massive with elongate green mottles perpendicular to the bedding, and has a zone (<2 cm) of dense, very dark red spots in one corner of the slab.

Sample N7 is a red mudstone similar to sample 18-2c. It also has a layer of alternating, light red and dark red laminations very similar to that of sample 18-2c.

Sample H5 is similar to sample H9 and is a structureless red mudstone. On the top surface of these two samples, are sub-circular cracks with average diameters of 2 cm. At first glance, these appear similar to mudcracks, but cracks are founded instead of polygonal, and edges curve downwards rather than upwards. Identification of these cracks is uncertain.

Unit 4E

Sample 1015-1 is a fine-grained, mauve doloarenite. Convex-upwards laminations are defined by alternating light and dark red bands. The walls of the stromatolites are fairly well-defined with massive mottled doloarenite occurring between stromatolites. A clear colourless, filled vug (2 x 1 mm) occurs on the side wall of one of the stromatolites.

APPENDIX 2

Thin Section Descriptions

Following are descriptions of 12 polished thin sections for which chemical analyses were also done. All rocks show complete recrystallization with a crystalline texture.

Slide B3 is intraclast-supported, coarse-grained and light coloured.

Intraclasts range in size from 1 cm by 1 mm, to .25 mm diameter. Grain size of the intraclasts is similar to that of the matrix between intraclasts but are darker in colour. Lenses of coarser-grained dolomite have inward-increasing grain size. Some of the larger intraclasts also contain coarser-grained vugs. Opaque, silt-sized, angular, quartz grains are rare. The presence of clay causes cloudy patches.

Slide B7 is light coloured, medium-grained, and generally even-textured with coarse-grained dolomite-filled vugs, .17 mm by 1.43 mm in size. A tiny clay chip .19 mm diameter, has a rough feathery rim. Small opaque grains are disseminated along a linear zone and a stylolite filled with clay, extends sinuously across the slide. No quartz grains were seen in this section.

Slide F3 is light coloured, has a fine-grained matrix, supporting lath-shaped grains (.039 by .013 mm), and has lenses of clear coarser grains. There are rare scattered spots of clay and rare, subrounded quartz grains, .039 mm in size.

Slide G7 is dark brown in colour and has a clay matrix supporting larger dolomite and quartz grains, .052 mm in size. Hematite specks occur throughout the matrix, with some larger patches showing its red brown colour. Quartz grains make up about 2% of the section.

Slide H1 is light coloured, with laminations of very fine-grained layers (.039 mm thick) alternating with coarse-grained layers (.12 mm thick). Pods or lenses of inward-expanding crystals are elongated in the direction of the lamination, and occur irregularly along the layers.

Styolites are filled with brown clay. Opaque, disseminated specks and subrounded, quartz grains are rare.

Slide H2 is light coloured, coarse-grained with finer-grained interlayers and discontinuous, clay laminations. Coarse-grained lenses, .26 by .16 mm in size, are scattered between the clay laminations. Opaque specks are disseminated throughout the slide, but may just be dirt in the slide. A patch of red hematite staining occurs along one of the clay laminations. Quartz grains are rare.

Slide H10 is light coloured, medium-grained with some fine-grained patches. Coarse grains (.32 mm), are supported in the medium-grained matrix. Clay is disseminated throughout the slide, but is not segregated into patches. Red hematite specks and quartz grains are rare.

Slide K2 is reddish brown in colour with hematite specks disseminated throughout the slide. The laminated, greenish clay matrix contains

larger dolomite and quartz grains. Quartz makes up 2% of the section.

Slide N1 is light coloured, medium-grained with a generally equigranular texture. One round, finer-grained, dark coloured intraclast (16 mm in diameter) is present in the slide. Clay is disseminated, but is not segregated into patches, and quartz grains are rare.

Slide N4 is light green coloured, intraclast-supported, with coarser-grained vugs between the intraclasts. Intraclasts are very fine-grained and range in size from .19 mm diameter to 1.5 by 2 mm. Discontinuous stylolites are filled with clay, and quartz grains are rare.

Slide N5 is light coloured with wispy red streaks. It is laminated with coarse and fine-grained layers. Opaque material occurs between grains in the coarser-grained layers. Quartz grains are <1% of the slide.

Slide L1 is light coloured and has irregular, fine, cloudy laminations with abundant lenses of clear, coarser grains. Opaque specks are disseminated throughout the slide. Hematite stains are rare, and no quartz was seen in this section.

APPENDIX 3

Wet Chemical Analysis

3a. Atomic Absorption

Analyses for the elements Ca, Mg, Al, Fe and Mn were done using standard wet chemical procedures and Atomic Absorption. Outline in Table A-1 (Appendix) is the sample digestion procedure used. This is the standard procedure used in the geochemical laboratory under the direction of W. Ervine at Dalhousie University.

Sample Solutions

To bring the concentration of the individual elements to levels detectable by the atomic absorption apparatus the following diluted solutions were prepared.

Ca: .5 ml of the resultant solution in step A (Table A-1) was diluted to 100 ml, thus a 200 times dilution.

Mg: .1 ml of the resultant solution in step A (Table A-1) was diluted to 100 ml, thus a 1000 times dilution.

Al: 40 ml of the resultant solution in step A (Table A-1) was diluted to 50 ml for all but 5 samples, thus a 1.25 times dilution.

For samples D2, G7, 18-2c, and N7, 25 ml of the solution in step A (Table A-1) were diluted to 50 ml, thus a 2 times dilution.

For sample K1, 15 ml of the solution in step A (Table A-1) were diluted to 50 ml, thus a 3.3 times dilution.

TABLE A-1

Whole-Rock AnalysisAnalyses in Aqueous SolutionsA. Sample Digestion

1. Accurately weigh approximately 0.5 gms of rock powder.
2. Put into Teflon cup and add approx. 0.5 ml H₂O. Stir to make uniform slurry.
3. Add 5 drops conc. HNO₃ and 20 ml of 1:4 mixture of HF and HClO₄.
4. Replace Teflon lids and heat gently in water bath over night. (Use copper top for water bath except for analyses for copper.)
5. Remove lids and turn heat to high. Leave until all HF and H₂O has evaporated (about 5 hours). The HClO₄ will remain.
6. Transfer cups to pre-heated sand bath. (Set dial at 6 to obtain a temperature of 250°C at bottom of sand). Let fume for 10 minutes.
7. Replace (dry) lids and leave covered for 30 minutes.
8. Remove lids and let fume until almost dry i.e. until a semi-liquid viscous residue is left in the cups. Let cool.
9. Add 5 ml HClO₄ and 25 ml H₂O.
10. Heat in water bath at boiling conditions for 1 hour. Let cool.
11. Transfer solution to a 250 ml volumetric flask. Wash the cups with H₂O and add washings to flask.
12. Make volume of flask with H₂O. Shake and transfer to plastic bottle. Label.

NOTE: Use safety equipment (rubber gloves, safety glasses, fume hood) except for weighing.

B. Sample Dilution

Pipette appropriate aliquots of sample rock solution into 100 ml plastic bottles. Add distilled water to bring the concentration of the elements into the following ranges:

Al: 10 - 50 ppm	Na: 0.2 - 1 ppm
Mg: 0.1 - 0.5	K : 0.4 - 2
Ca: 1 - 5	Mn: 1 - 3
Fe: 1 - 5	

C. Preparation of Standard Solutions

Dilute the Fisher Stock Standard Solutions to obtain a series of working standard solutions in the range of each element shown above.

D. Preparation of Blank Solutions

Prepare blank solutions in a manner identical to the sample digestion except that no rock powder is used.

E. Preparation of 5% La Solution

All working solutions (sample, standards, and blanks) must contain 20 ml of 5% La solution for every 100 ml of working solution. It is prepared by mixing 58.64 gm La₂O₃ with 50 ml H₂O. Then slowly add 250 ml conc. HCl. Let cool. Dilute to 1000 ml with distilled water.

Mn: No dilutions were necessary

Fe: No dilutions were necessary

Standard Preparations

Ca and Fe standards were prepared by diluting 10 ml portions of 1000 ppm commercial standards for Ca and Fe, to 100 ml. Five standard solutions for both elements were prepared by taking 1 ml, 2 ml, 3 ml, 4 ml, and 5 ml, of the previous diluted solution and diluting to 100 ml. This gave standard Ca and Fe solutions with 1 γ , 2 γ , 3 γ , 4 γ and 5 γ in 1 ml.

Mg standards were prepared by diluting 1 ml of 1000 ppm commercial standard for Mg, to 100 ml. Five standard solutions were prepared by diluting 1 ml, 2 ml, 3 ml, 4 ml and 5 ml, of the previously diluted solution, to 100 ml. This gave standard Mg solutions with .1 γ , .2 γ , .3 γ , .4 γ , and .5 γ in 1 ml.

All standards were prepared by diluting 1 ml, 2 ml, 3 ml, 4 ml and 5 ml portions of 1000 ppm commercial Al standard and diluting each to 100 ml. This produced standard Al solutions with 10 γ , 20 γ , 30 γ , 40 γ , and 50 γ in 1 ml.

Mn standards were prepared by diluting 10 ml of 1000 ppm commercial Mn standard, to 100 ml. Five standard solutions were prepared by diluting 1 ml, 1.5 ml, 2 ml, 2.5 ml and 3 ml portions of the previously diluted solution, to 100 ml. This produced Mn standard

solutions with 1 γ , 1.5 γ , 2 γ , 2.5 γ and 3 γ in 1 ml.

Atomic Absorption

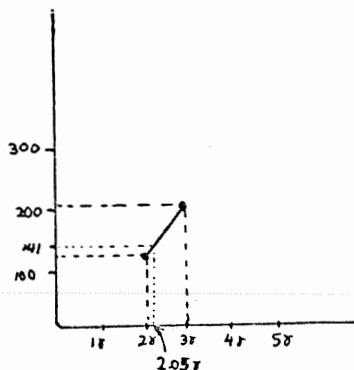
Standard blank, 5 standards, sample blank and 30 samples were run three times consecutively for each element using the lamp, burner and settings recommended in the manual for each element. The absorption readings were tabulated and the weight percent of each element was calculated.

Wt% Calculation

The wt% for each element was calculated by comparing the sample atomic absorption readings with those of the standard solutions, taking the various dilution factors into account, and comparing with the original weight of the sample. A sample calculation for the Ca wt% of sample H1 follows.

Atomic Absorption for Run #1 for H1 is 141. This is between the standard solution 2 γ with 137 and 3 γ with 209.

Plot 2 γ and 3 γ on a graph against their atomic absorption readings and connect the two points. See figure below.



Follow the H1 absorption reading, 141, horizontally on the graph until it intersects the line joining 2 γ and 3 γ standards. At this point drop vertically to read the number of γ in sample H1. This is 2.05 γ . Do this for each of the 3 runs and then average.

The average for H1 is 2.04 γ in 1 ml. To find the number of γ of Ca in the original sample multiply by the number of times dilutions the original sample underwent before being run for atomic absorption.
i.e. sample diluted to 250 ml = 250 times dilution

.5 ml diluted to 100 ml = 200 times dilution

total dilution = 250 x 200

$\therefore 2.04 \times 250 \times 200 = 102,000\gamma$ or 102 mg Ca in original solution

original sample weight = .499 g

$\frac{102 \text{ mg}}{499 \text{ mg}} \times 100 = 20.44\% \text{ Ca}$

499 mg

Values are traditionally recorded as CaO wt%

$\therefore .102 \text{ g}$ is .0025 moles of Ca, this reacts with .0025 moles of

O = .04 g

\therefore CaO weighs .142 g

$\frac{.142}{.499} \times 100 = 28.45\% \text{ CaO}$. This value is tabulated in Table 3.

.499

Ca/Mg Ratio

Calculate % Ca without the oxygen attached. e.g. Sample H1.

$$\frac{\text{CaO}}{\text{Ca}} = 1.39 \quad \frac{28.4}{\text{Ca}} = 1.39, \quad \text{Ca} = 20.44\%$$

20.44 g Ca is .510 moles \therefore .510 mole %Ca

Calculate Mg without the oxygen attached.

$$\frac{\text{MgO}}{\text{Mg}} = \frac{40.31}{24.31} = 1.66$$

$$\therefore \text{Mg} = \frac{21.55}{1.66} = 12.80\%$$

12.80 g Mg is .526 moles \therefore .526 mole %Mg

$$\text{Ca/Mg} = .969$$

3b. CO₂ Analysis
Acid-Base Titration

Procedure

CO₂ analysis was done by acid-base titration following the procedure outlined by Grimaldi et al. (1966).

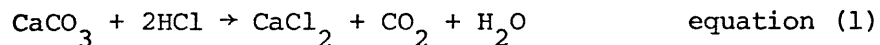
25 ml of water and 50 ml from a buret of 0.2 N HCl were added to a 250 ml beaker containing approximately .5 g of powdered sample. The mixture was boiled until the evolution of CO₂ was complete, about 5 minutes. Several grams of ammonium chloride were added to keep ferrous iron in solution. 8 to 10 drops of .01 W/V bromphenol blue indicator were added and the solution was titrated with 0.2 N NaOH to the blue end point past the last green tinge. Samples with considerable dark red insoluble residue were filtered before back titrating allowing better visibility of the blue end point.

In order to determine the exact strength of the HCl solution prepared, 50 ml of the .2N HCl was titrated with .2N NaOH. The result was an average of 61.25 ml after 4 titrations.

61.25 ml NaOH neutralized 50 ml HCl

The above procedure was carried out for a standard limestone sample with 44% CO₂ to test the accuracy of the procedure. The result was 43.43% CO₂.

Sample Calculation of % CO₂



∴ 2 moles of HCl produces 1 mole of CO₂

50 ml HCl was present at the beginning of the reaction. This is equivalent to 61.25 ml NaOH according to the above neutralizing test. After the reaction, x ml of NaOH were needed to neutralize the remaining unreacted HCl. Therefore the HCl used during the reaction is (61.25 - x) ml.

To obtain the number of grams of CO₂ in the sample:

According to equation (1) 1 litre 1N HCl produces 1/2 mole CO₂ = 22 gm

1 litre 0.2 N HCl produces 4.4 gm CO₂

1 ml 0.2N HCl is equivalent to .0044 gm CO₂

∴ (61.25 - x) ml HCl is equivalent to (.0044) (61.25 - x) gm

∴ there are (61.4 - x) (.0044) gm of CO₂ in the original sample.

To obtain the percent CO₂ in original sample, divide the number of grams CO₂ in the sample by the total weight of the original sample times 100.

$$\frac{61.4 - x)(.0044)}{\text{sample wt}} \times 100 = \text{wt\% CO}_2$$

APPENDIX 4

Determination of minerals using x-ray diffraction

Quartz is the only mineral which can be definitely identified from the peaks shown on the x-ray diffraction graphs. The other minerals have been identified by the process of elimination of other minerals with critical peaks missing. Even then, the mineral identified does not fit exactly but is the best choice with the data available.

Outlined below is the process used to determine the minerals.

On the unprocessed sample graph:

For the peak at 25.5 possible minerals are chlorite and vermiculite.

Chlorite: - high intensity peak at 25.5 is present, slightly lower intensity peaks should be at 18.4-18.8, 12.3-12.7, and 6.2-6.5. However these peaks here are only slightly above background.

Vermiculite: - medium intensity peak at 25.5 is present, at 19.3 there should be a peak of a similar intensity to that at 25.5. This peak is not present.

the most likely mineral represented at peak 25.5 is chlorite.

For the peak at 26.7 the mineral is quartz. Its other major peak is present at 20.8.

For the peak at 26.75 orthoclase and illite are possibilities.

Orthoclase: - should have a medium peak at 27.2. This may be masked by the 27.4 peak. Its major peak at 26.75 is present.

Peaks at 23.4 and 22.5 are present but their relative intensities are reversed. The 13.6-14.1, which should be a low to medium intensity peak, is not present.

Illite: - Its high intensity peak at 26.75 is present. There should be a high intensity peak at 19.7-19.8. There is only a low intensity peak here. The most intense peak should be at 8.7-8.9. No peak occurs here.

The peak at 26.75 is probably not illite and by elimination must be Orthoclase.

For the peak at 29.6 the minerals muscovite and calcite are possible.

Muscovite: - the 29.8 peak for muscovite is only a medium peak. Its major peak is at 26.75 which is present. Peaks also occur at 25.5, and at 19.7. However this 19.7 peak should be of high intensity and here is just above background. An intense peak should be at 8.7-8.9. This is not present. Therefore judging by the lack of those large peaks the mineral is not muscovite.

Calcite: - Its most intense peak is 29.4 which may be the 29.6 peak. No other major peaks are listed in Piper (1977) for the interval of 30 20 .

From this information it appears that the mineral at 29.6 is calcite.

However, examining the insoluble residue graph, a similar peak for calcite? occurs. This could not be calcite in this as calcite

could not survive the boiling treatment in HCl which this sample underwent. Therefore one is back to the mineral muscovite which then suggests that chlorite and orthoclase are not present.

For the peak at 30.7 dolomite is the only possible mineral. This peak is also present in the insoluble residue sample which means that some dolomite survived the boiling HCl acid treatment. (This leads to some doubt about the accuracy of insoluble residue results.)

For the peak at 27.5 on the insoluble residue graph plagioclase and palygorskite are possible.

Palygorskite: - has a maximum at 27.6 which is present, the smaller peak at 25.5 is present, a medium peak at 21.0-21.2 is not present. Another maximum at 8.4-8.7 is not present in sufficient intensity. The mineral then is unlikely to be Palygorskite.

Plagioclase: - The maximum peak at 27.8 is present although at 27.8 instead of at 27.8. A small peak at 13.6-14.1 is present. Peaks at 22.3 and 23.4 are present but their relative intensities are reversed. The 22.3 peak should be much larger.

Although it does not fit the data perfectly plagioclase seems the most likely mineral for the peak at 27.5.

By measuring the area under each of the maximum peaks and multiplying this by the intensity factor listed on p. 82 (Piper, 1977) the relative abundances of the minerals can be obtained.

Therefore, following the above assumption the minerals and their approximate abundances as indicated from the x-ray diffraction data available are:

Chlorite?	3 %
Dolomite	.9%
Orthoclase?	14.3%
Plagioclase	5 %
Quartz	9 %
Muscovite	12 %

Peaks may be masked or reduced by interference of other undetected minerals. The clay minerals may be masked here by the higher intensity minerals. A special procedure would be necessary to detect the clay minerals specifically.

